Available online at www.sciencedirect.com

ScienceDirect

Geochimica et Cosmochimica Acta 143 (2014) 143–164

Geochimica et Cosmochimica Acta

www.elsevier.com/locate/gca

Geochemistry of primary-carbonate bearing K-rich igneous rocks in the Awulale Mountains, western Tianshan: Implications for carbon-recycling in subduction zone

Wu-Bin Yang [a], He-Cai Niu [a,*], Qiang Shan [a], Hua-Yong Chen [a], Pete Hollings [b], Ning-Bo Li [a,c], Shuang Yan [a,c], Robert E. Zartman [a]

[a] *Key Laboratory of Mineralogy and Metallogeny, Guangzhou Institute of Geochemistry, Chinese Academy of Sciences, Guangzhou 510640, PR China*

[b] *Department of Geology, Lakehead University, 955 Oliver Road, Thunder Bay, Ontario P7B 5E1, Canada*

[c] *Graduate University of Chinese Academy of Sciences, Beijing 100049, PR China*

Available online 5 May 2014

Abstract

Arc magmatism plays an important role in the recycling of subducted carbon and returning it to the surface. However, the transfer mechanisms of carbon are poorly understood. In this study, the contribution of subducted carbonate-rich sediments to the genesis of the carbonate-bearing K-rich igneous rocks from western Tianshan was investigated. Four key triggers are involved, including sediments subduction, slab decarbonation, partial melting and magma segregation. The globular carbonate ocelli show C–O isotope signatures intermediate between oceanic sediments and mantle, suggesting that the carbon of the primary carbonate ocelli was derived from recycled subducted sediments in the mantle. Decarbonation of the subducted slab is regarded as the primary agent to carbonize the mantle wedge. Geochemical features indicate that the carbonate ocelli are primary, and that the parental K- and carbon-rich mafic alkaline magma was derived from partial melting of carbonated mantle wedge veined with phlogopite. Major and trace element compositions indicate that globular carbonate ocelli hosted in the Bugula K-rich igneous rocks are calcio-carbonate and formed primarily by segregation of the differentiated CO_2-rich alkaline magma after crystallization fractionation. The K-rich alkaline magma, which formed from partial melting of metasomatized (i.e., phlogopite bearing) mantle wedge in the sub-arc region, is a favorable agent to transport subducted carbon back to the Earth's surface during carbon recycling in subduction zones, because of the high CO_2 solubility in alkaline mafic magma. We therefore propose a model for the petrogenesis of the carbonate-bearing K-rich igneous rocks in western Tianshan, which are significant for revealing the mechanism of carbon recycling in subduction zones.

1. INTRODUCTION

It is estimated that each year subduction transports approximately 20 km^3 of oceanic crust into the mantle (Zhang et al., 2012a) with 2.3–3.7 $\times 10^{12}$ mol of carbon (Dasgupta et al., 2004), most of which is carried into the deep mantle (Hofmann, 1997; Sleep and Zahnle, 2001; Dasgupta, 2013) whereas the remainder contributes to mantle wedge metasomatism by slab decarbonation and/or melting processes. Arc and mid-ocean-ridge volcanism are the predominate mechanisms for removing the subducted carbon from the deep mantle (Sano and Williams, 1996; Sleep and Zahnle, 2001). Primary carbonate melts and carbon-bearing silicate melts have been proposed as important mechanisms for liberating carbon from the mantle wedge (Gorman et al., 2006; Dasgupta et al., 2013).

* Corresponding author.
E-mail address: niuhc@gig.ac.cn (H.-C. Niu).

http://dx.doi.org/10.1016/j.gca.2014.04.033
0016-7037/

Previous studies have documented that partial melting of subducted sediments produce vein networks of clinopyroxene/amphibole/phlogopite minerals within the subcontinental lithospheric mantle (Pilet et al., 2008; Hermann and Rubatto, 2009; Skora and Blundy, 2010). Partial melting of those pure vein minerals will generate ultrapotassic magmas, whereas increasing interaction between these veins and the surrounding mantle will decrease the alkaline component and result in relatively low-K shoshonites and calc-alkaline rocks (Avanzinelli et al., 2009; Conticelli et al., 2009a,b). This genetic model has been applied to shoshonitic series rocks associated with ultrapotassic rocks, high-K calc-alkaline rocks, and even to calc-alkaline rocks (e.g., Duggen et al., 2005; Altherr et al., 2008; Avanzinelli et al., 2009; Conticelli et al., 2009a).

It has been proposed that primary carbonate melt can be generated from direct melting of carbonate-bearing mantle peridotite (Sweeney, 1994; Ray et al., 1999; Lee et al., 2000; Woolley, 2003), liquid immiscibility from an initially homogeneous CO_2-rich alkaline silicate magma (Hamilton et al., 1979; Kogarko et al., 1995; Brooker and Kjarsgaard, 2011), or extensive fractional crystallization of a carbonated or CO_2-rich alkaline silicate magma (Watkinson and Wyllie, 1971; Dasgupta et al., 2007; Zeng et al., 2010; de Ignacio et al., 2012). However, the origin of carbonate melts and their relationship to associated silicate rocks is still controversial. In subduction zones, Sr–Nd–Pb and C–O isotopes have been interpreted to indicate that most carbonate melts associated with alkaline igneous rocks were derived from the recycling of subducted carbonate-rich sediments (e.g., Bell and Simonetti, 1996; van Achterbergh et al., 2002; Walter et al., 2008; Marin-Ceron et al., 2010; Frezzotti et al., 2011). Therefore, the occurrence and genesis of primary carbonate-bearing K-rich igneous rocks in the convergent margins can be utilized to help understanding crust–mantle interaction and can provide insights into the mechanisms of carbon-recycling within the mantle wedge during subduction. In this study, we discuss the origin of primary-carbonate aggregations in the K-rich igneous rocks from the Awulale Mountains, western Chinese Tianshan. Comprehensive geochemical and isotopic data of both K-rich igneous rocks and carbonate are used, in order to better understand the petrogenesis of these rocks and the implications for recycling of subducted carbonates.

2. GEOLOGICAL SETTING AND SAMPLE DESCRIPTIONS

2.1. Regional geology

The Kazakhstan–Yili plate in western Chinese Tianshan is sandwiched between the northern and southwestern Tianshan orogenic belts and widens westwards into Kazakhstan (Fig. 1a). The Awulale Mountains are located among the intersection of the Junggar, Tarim and Kazakhstan–Yili plates, and form part of the Central Asia Orogenic Belt (CAOB). It is mainly comprised of Late Paleozoic volcanic and intrusive rocks (Fig. 1b). Numerous Fe–Cu (Au) polymetallic deposits were recently reported from here (Luo et al., 2009; Shan et al., 2009; Zhao et al., 2009) in the so-called Awulale Fe–Cu Metallogenetic Belt (Zhang et al., 2012b). The northern Tianshan fault divides the Yili plate from the northern orogenic belt, whereas the north Nalati fault forms the south boundary with the southwestern Tianshan orogenic belt (Fig. 1b).

Late Paleozoic igneous rocks formed during the subduction of the Tianshan oceanic plate subduction northward under the Kazakhstan–Yili plate are widely distributed in the western Tianshan along the southwestern margin of the CAOB (Gao et al., 2009; Xiao et al., 2010; Wang et al., 2011; Yang et al., 2012). The occurrence of Carboniferous–Permian potassic and ultrapotassic igneous rocks associated with Cu–(Au) mineralization in the Awulale Mountains has been interpreted to be the result of a fundamental shift of geodynamic setting associated with the termination of subduction (Zhao et al., 2009; Pirajno et al., 2011; Yang et al., 2012; Xiao et al., 2013). Generally, the Awulale Mountains can be divided into two sections based on the regional lithology. The western section is mainly composed of Permian volcanic rocks (251–298 Ma) and some Late Paleozoic intrusive rocks, whereas, the eastern section is composed of Carboniferous volcanic rocks (312–327 Ma), some Late Paleozoic intrusive rocks (284–312 Ma) and a few Permian volcanic rocks (261–271 Ma) (Fig. 1b).

The Dahalajunshan Formation is composed of a suite of volcanic-sedimentary rocks, consisting of rhyolite, trachyte, trachyandesite and ignimbrite, with a thickness of 7500–9000 m (Zhu et al., 2006). The lower section is dominated by andesite breccia, dacitic tuff, ignimbrite and basaltic andesite, whereas the upper section is composed of thick andesitic tuff breccia, dacitic crystal tuff, dacite and K-rich trachyandesite. The K-rich igneous rocks in the Bugula region investigated in this study were intruded as shallow plutons into the upper section of the Dahalajunshan Formation. K-rich igneous rocks of the Dahalajunshan Formation are also present in the Yuximolegai and south Yuximolegai regions, located to the east of Bugula (Fig. 1b). The K-rich igneous rocks in the Yuximolegai region are mainly composed of basaltic trachyandesite and trachyandesite (Yang et al., 2012), whereas the K-rich igneous rocks from south Yuximolegai are trachybasalt and basaltic trachyandesite (Sun et al., 2008). Combined with the globular carbonate hosted in the Bugula K-rich igneous rocks, calcite veins associated with Cu (Au)-mineralization in Yuximolegai, Chagangnuoer and Wulangdaban from both eastern and western sections of the Awulale Mountains (Fig. 1b) were also investigated in this study.

2.2. Sample descriptions

The Bugula K-rich igneous rocks are composed of 15–20 vol.% phenocrysts, 1–3 vol.% globular carbonate and groundmass. Phenocrysts are dominantly composed of K-feldspar, clinopyroxene, olivine and minor phlogopite (Fig. 2). The matrix is mainly composed of intergranular pyroxene, K-feldspar, and minor magnetite, with secondary sericite and chlorite. Some K-rich igneous rocks contain numerous millimetre- to centimetre white polycrystalline globular carbonate phenocrysts, called ‘ocelli’ elsewhere by Phillips (1973) and Foley (1984), set in a dark-green mafic

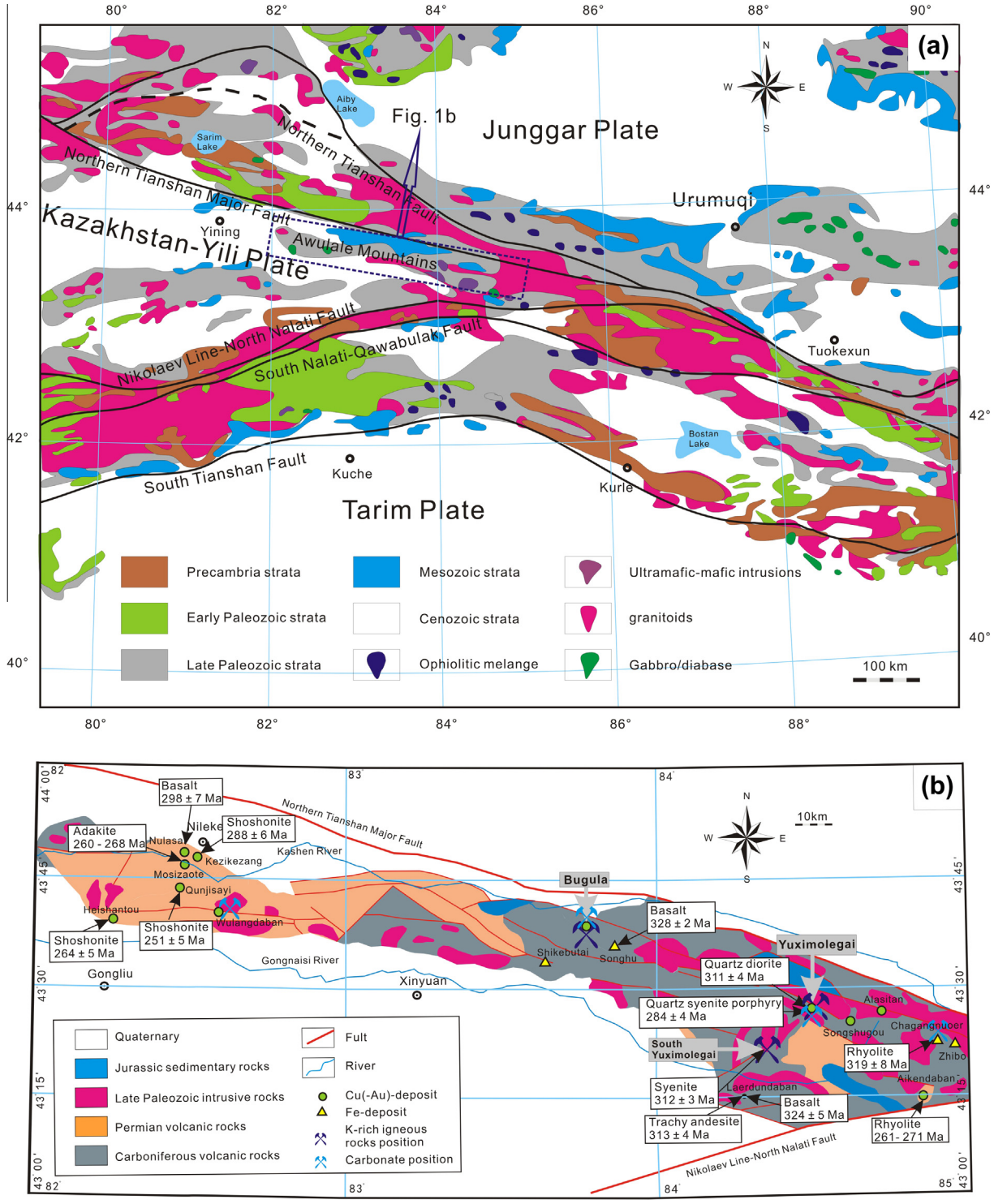

Fig. 1. Geological maps of the western Chinese Tianshan (a) and the Awulale Mountains (b), modified from Gao et al. (2009). The labeled geochronological data in Fig. 1b are from references (Li et al., 1997; Chen et al., 2004; Sun et al., 2008; Zhao et al., 2009; Zhu et al., 2009; Yang et al., 2012).

matrix (basaltic host). The presence of local olivine and the preservation of quenched textures in some carbonate globules (Fig. 2a) suggest that the carbonate is magmatic in origin. Some parts of the white ocelli are nearly pure crystalline calcite (Fig. 2b), whereas others include silicate minerals (Fig. 2c and d). Both carbonate and silicate melt inclusions have been identified in the globular calcite (Fig. 2e and f), which are consistent with a primary of magmatic origin.

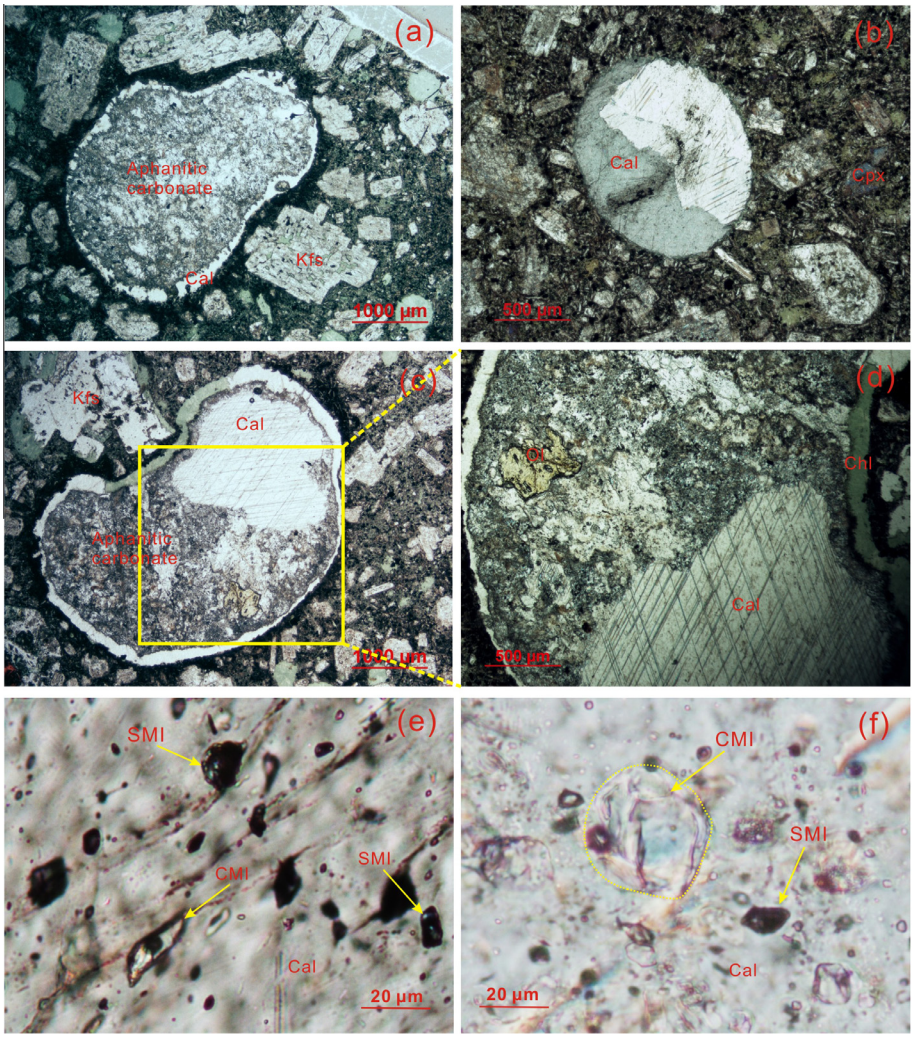

Fig. 2. Photomicrographs of selected samples from Bugula. (a) Globular aphanitic carbonate ocellus with quenched textures. (b) Globular calcite ocellus in K-rich basaltic rocks. (c and d) Aphanitic carbonate, calcite, and olivine coexist in a carbonate globule. (e and f) Silicate melt inclusions (SMI) and carbonate melt inclusions (CMI) in globular carbonate, suggesting that the carbonate globules are primary and formed at high temperature. *Abbreviations:* Cal–calicite, Chl–chlorite, Kfs–K-feldspar, Cpx–clinopyroxene, Ol–olivine.

Sericitization of K-feldspar and chloritization of clinopyroxene and olivine are consistent with the Bugula K-rich igneous rocks having undergone low intensity hydrothermal alteration. Olivine is also replaced by iddingsite in some samples. Chlorite rims can be observed on the margin of some carbonate globules. The Bugula K-rich alkaline basalts can be classified as plagioleucitites, based on major element compositions. Leucite, however, has not been observed in the Bugula alkaline basalts, probably because they can be easily transformed into analcime and other clay minerals during alteration (Giampaolo et al., 1997; Putnis et al., 2007).

3. ANALYTICAL METHODS

Both major and trace element compositions were analyzed at the Guangzhou Institute of Geochemistry, Chinese Academy of Science (GIGCAS). Unaltered or least-altered samples were selected by optical microscopy for geochemical analysis. The basalt samples were crushed to 1–5 mm chips and the white carbonate hand-picked under a binocular microscope. The selected basalt samples were powdered to less than 200 mesh by using an agate mortar for whole-rock trace element and isotope analyses. Major element oxides were determined using the X-ray fluorescence method of Li et al. (2005). Loss-on-ignition was obtained by determining the weight loss of samples ignited in a furnace at 900 °C for 2 h and allowed to cool in a desiccator to minimize moisture absorption, which can be a major source of error in carbonate LOI determination. Approximately 50 mg of powdered whole-rock sample was dissolved in high-pressure Teflon bombs with a mixture of $HF + HNO_3$. Trace elements were analyzed by inductively coupled plasma mass spectrometry, using a Perkin-Elmer Sciex ELAN 6000 instrument following the analytical procedures described by Liu et al. (1996).

Rhodium was used as an internal standard to monitor signal drift during counting. Analytical precision for most elements is better than 3%.

The separated carbonates were analyzed by a Perkin-Elmer Sciex ELAN 6000 at GIGCAS. Carbonate samples were crushed to 1 mm in size, sieved and washed, and then handpicked for analyses. Fifty miligrams of powder was dissolved in a Teflon bomb using 1 ml of HF (38%) and 0.5 ml of HNO_3 (68%). The sealed bomb was heated to 190 °C for 12 h. One milliliter of 1 μg/ml Rh was added to the cooled solution as the internal standard and the solution was then evaporated. One ml of HNO_3 (68%) was added, evaporated to dryness and the process repeated. The final residue was re-dissolved in 8 ml of HNO_3 (40%). The bomb was sealed and heated to 110 °C for 3 h. The final solution was diluted to 100 ml by addition of distilled de-ionized water for ICPMS analysis. Precision of analytical results as estimated from replicate measurements was better than 10% RSD. The details of this procedure are given in Li (1997).

For Sr–Nd isotope determination, sample powders were firstly dissolved in Teflon capsules with $HF + HNO_3$ acid. Strontium and REE were separated using cation columns, and then the Nd fractions were further separated using HDEHP-coated Kef columns. Isotopic measurement was performed on the Micromass Isoprobe multicollector mass spectrometer at GIGCAS, following analytical procedures described by Wei et al. (2002) and Liang et al. (2003). Measured $^{87}Sr/^{86}Sr$ and $^{143}Nd/^{144}Nd$ ratios were normalized to $^{86}Sr/^{88}Sr = 0.1194$ and $^{146}Nd/^{144}Nd = 0.7219$, respectively. The reported $^{87}Sr/^{86}Sr$ and $^{143}Nd/^{144}Nd$ ratios were respectively adjusted to the NBS SRM 987 standard with an $^{87}Sr/^{86}Sr$ value of 0.71025 and the Shin Etsu JNdi-1 standard with a $^{143}Nd/^{144}Nd$ value of 0.512115.

Lead was separated and purified by a conventional cation-exchange technique (AG1 8, 200–400 resin) with diluted HBr and HCl used as the eluants. The Pb isotopic ratios were measured using a VG-354 mass-spectrometer at the GIGCAS following procedures described by Zhu et al. (2001). Analytical uncertainties expressed as 2σ for Pb isotopic ratios are better than 0.1%.

Stable isotopes analysis of carbon and oxygen were carried out on a VG IsoPrime II mass spectrometer at GIGCAS. CO_2 was liberated from ca. 20 mg samples by reaction with 100% phosphoric acid in a vacuum, and the gas analyzed for O and C isotopes. Analytical uncertainties are better than ±0.08% for $\delta^{18}O$ (reported relative to SMOW) and ±0.05% for $\delta^{13}C$ (relative to PDB).

4. RESULTS

4.1. Major and trace element chemistry of the K-rich igneous rocks

The Bugula K-rich igneous rocks have relatively low SiO_2 contents (47–58 wt.%) and high Al_2O_3 (15–21 wt.%) (Table 1). They are characterized by $K_2O > 2.9$ wt.%, MgO > 1.7 wt.% and K_2O/Na_2O ratios from 0.56 to 8.46, consistent with all of the Bugula K-rich igneous rocks being ultrapotassic and potassic based on the criteria of Foley et al. (1987). On an $Na_2O + K_2O$ versus SiO_2 classification diagram (Lebas et al., 1986) the Bugula K-rich igneous rocks lie almost totally within the tephrite–phonotephrite–basaltic trachyandesite fields, whereas the K-rich igneous rocks from Yuximolegai and south Yuximolegai plotted in the trachybasalt–basaltic trachyandesite–trachyandesite fields (Fig. 3a). A plot of K_2O versus SiO_2 shows that most of the K-rich igneous rocks in the Awulale Mountains belong to the shoshonitic magma series (Fig. 3b).

The K-rich igneous rocks have Mg-numbers [molar $Mg \times 100/(Mg + 0.85 \times FeO_{tot})$] ranging from 25 to 64 (Table 1). The SiO_2 contents increase, whereas Fe_2O_3, Ni, Co and Cr decrease, with decreasing MgO contents (Fig. 4). This may be explained by fractional crystallization of olivine and clinopyroxene, which is consistent with petrographical observations. However, no correlations exist between abundances of incompatible trace elements (e.g., Rb, Sr, Nb, Zr and Pb) and MgO (Table 1). LOI values in K-rich igneous rocks usually reflect the presence of hydrous mineral phases (e.g., phlogopite), carbonates and/or secondary minerals (e.g., chlorites) (Guo et al., 2006; Labanieh et al., 2012). The elevated LOI values (2.4–6.3 wt.%) in Bugula K-rich igneous rocks are likely the result of primary carbonate globules and small amounts of phlogopite and chlorites according to our petrological observations. However, there is no correlation between LOI and La/Sm ratios in Fig. 5 for the K-rich rocks from the Awulale Mountains, suggesting that alteration did not create changes in the ratio of LREE to MREE (e.g., Labanieh et al., 2012). This observation is consistent with the relatively immobile behavior of the REE during hydrothermal or metamorphic fluid–rock interaction at low fluid/rock ratios as described by Bau (1991) and Labanieh et al. (2012).

Chondrite-normalized REE patterns (Fig. 6a) and primitive mantle-normalized incompatible element diagrams (Fig. 6c) for the Bugula samples show strong incompatible element enrichment. The Bugula K-rich igneous rocks are characterised by enriched light REE (LREE), relatively flat heavy REE (HREE) profiles (chondrite-normalized La/Yb and Dy/Yb ratios are 1.07–8.99 and 1.39–2.29, respectively) and slightly negative Eu anomalies (Fig. 6a). Similar REE patterns have been reported for plagioleucitites from NE Turkey (Altherr et al., 2008) and leucite-bearing K-rich igneous rocks from central Italy (Boari et al., 2009). Total REE of the Bugula K-rich igneous rocks range from 13.6 to 104 ppm, significantly lower than those of the plagioleucitites from NE Turkey (1164–1748 ppm) (Altherr et al., 2008) and also those of K-rich igneous rocks from central Italy (460–1063 ppm) (Boari et al., 2009), with lower chondrite-normalized La/Sm and La/Yb ratios ranging from 0.59 to 2.61 and from 0.76 to 6.45, respectively (Table 1). Trace element concentrations range from several times primitive mantle for heavy REE (HREE), Ti and Y, to several hundred times for large ion lithophile elements (LILE) such as Rb, Ba, Th, U, K and Pb (Fig. 6c). The mantle-normalized incompatible trace element patterns are distinguished by negative Nb–Ta–Ti and positive Pb anomalies (Fig. 6c), which are features of magma derived from suprasubduction zones (e.g., Foley et al., 1987; Altherr et al., 2008; Boari et al., 2009).

Table 1
Major and trace element compositions of the Bugula K-rich igneous rocks in Awulale Mountains.

Sample	BG'082-4	BG'083-4	BG08-10	BG08-17	BG08-8B	BG7-1Cu	BG7-2Cu	BG7-3Cu	BG8	BG9
SiO_2	54.43	53.29	48.18	53.18	50.59	54.36	52.91	54.57	47.49	49.36
TiO_2	0.80	0.91	0.80	0.83	0.80	0.78	0.76	0.79	0.72	0.82
Al_2O_3	19.50	19.19	18.42	20.44	19.33	19.27	18.98	19.18	16.85	17.35
Fe_2O_3T	10.83	12.60	16.02	8.21	9.65	10.20	11.05	10.16	15.41	14.33
MnO	0.13	0.18	0.33	1.31	1.51	0.60	0.66	0.59	0.46	0.79
MgO	3.46	4.06	6.80	4.58	7.39	4.03	4.35	4.03	7.54	7.97
CaO	1.52	0.82	1.94	3.27	2.29	2.45	2.75	2.35	4.14	1.24
Na_2O	5.83	5.61	3.72	4.41	3.12	4.64	5.26	4.64	1.76	5.09
K_2O	3.38	3.21	3.61	3.64	5.16	3.53	3.15	3.55	5.48	2.87
P_2O_5	0.13	0.14	0.19	0.15	0.16	0.14	0.14	0.14	0.15	0.19
LOI	2.40	3.01	4.83	3.37	3.82	3.77	4.19	3.87	6.34	3.24
K	28015	26643	29938	30184	42780	29288	26099	29462	45503	23789
Sc	34.75	30.45	34.43	31.78	38.7	29.22	29.00	28.81	37.6	34.9
Ti	5317	5813	4592	4631	4762	4238	4175	4226	3710	4396
V	245	363	276	241	260	234	225	229	216	319
Cr	18.62	6.04	67.04	28.12	50.6	23.91	27.28	23.32	214	90
Mn	1294	1646	2660	10877	12822	4100	4457	3986	3272	5503
Co	27.64	27.24	37.91	28.84	48.8	23.49	25.52	23.17	37.9	46.1
Ni	5.37	1.50	32.73	14.80	22.5	9.64	9.74	9.67	55.1	37.1
Cu	5.70	4503	21.48	65.16	2.62	49.05	158.80	24.25	8.2	40.5
Zn	29.94	27.83	65.65	389	637	182	198	183	156	288
Ga	19.78	20.26	17.95	19.89	19.5	18.23	17.90	17.61	15.4	16.4
Ge	2.11	1.55	1.76	1.55	1.44	1.26	1.54	1.55	1.76	1.44
Rb	97.53	68.40	77.30	111	119	132	107	130	181	43.4
Sr	291.00	88.59	86.92	355	360	235	218	220	93.4	65.3
Y	19.32	18.31	14.32	15.73	15	16.37	16.24	16.40	15.8	13.8
Zr	62.95	63.99	53.36	59.71	55.1	54.84	52.92	55.11	42.7	50.4
Nb	2.54	2.76	2.02	2.42	2.09	2.16	2.09	2.20	1.49	1.82
Cs	\	\	\	\	\	6.35	3.62	5.47	4.16	1.94
Ba	1401	861	1108	2320	4259	1117	1081	1070	1571	537
La	18.65	2.12	5.94	6.98	9.74	5.93	6.01	6.19	8.92	4.28
Ce	38.60	5.32	12.74	16.18	22	14.42	14.07	15.27	20.4	10.8
Pr	4.84	0.81	2.01	2.38	3.19	2.14	2.07	2.31	2.96	1.68
Nd	20.49	4.89	9.11	10.61	14.5	9.84	9.36	10.12	12.9	7.65
Sm	4.61	2.33	2.69	2.77	3.27	2.55	2.53	2.55	3.46	2.18
Eu	1.85	0.92	1.00	1.02	1.46	0.85	0.69	0.87	1.22	0.56
Gd	4.35	2.99	2.83	2.86	3.15	2.82	2.82	2.85	3.52	2.36
Tb	0.68	0.56	0.52	0.51	0.51	0.49	0.50	0.51	0.59	0.44
Dy	3.93	3.52	2.99	3.08	2.91	3.31	3.23	3.19	3.36	2.65
Ho	0.89	0.73	0.61	0.67	0.62	0.70	0.69	0.69	0.65	0.55
Er	2.28	2.12	1.66	1.85	1.72	2.00	1.99	1.94	1.7	1.59
Tm	0.34	0.32	0.23	0.27	0.26	0.30	0.29	0.28	0.23	0.23
Yb	2.07	1.99	1.45	1.77	1.64	1.90	1.87	1.81	1.47	1.56
Lu	0.33	0.32	0.23	0.30	0.26	0.29	0.31	0.29	0.22	0.24
Hf	2.06	1.88	1.60	1.86	1.61	1.88	1.75	1.83	1.45	1.55
Ta	0.17	0.18	0.13	0.17	0.14	0.18	0.17	0.18	0.12	0.13
Pb	1.72	1.46	4.73	16.81	5.33	5.76	5.73	3.13	2.51	2.51
Th	1.58	1.77	1.86	1.70	2.01	1.80	1.69	1.78	1.82	1.69
U	0.42	0.70	0.57	0.48	0.67	0.57	0.48	0.53	0.57	0.55
Mg#	43	43	50	57	64	48	48	48	53	56
$K_2O + Na_2O$	9.20	8.82	7.32	8.05	8.28	8.17	8.41	8.19	7.25	7.96
K_2O/Na_2O	0.58	0.57	0.97	0.82	1.65	0.76	0.60	0.77	3.11	0.56
La/Sm	4.05	0.91	2.21	2.52	2.98	2.33	2.38	2.43	2.58	1.96
Ba/Th	887	486	597	1368	2119	622	641	600	863	318
La/Yb	8.99	1.07	4.09	3.94	5.94	3.12	3.22	3.42	6.07	2.74

(*continued on next page*)

Table 1 (*continued*)

Sample	BG7-1K	BG7-2K	11BG01-1	11BG07-1	11BG07-2	11BG07-3	11BG08-1	11BG11-1	11BG13-1	11BG14-1
SiO_2	56.88	51.70	57.83	49.58	48.58	51.82	53.68	52.00	52.59	53.65
TiO_2	0.70	0.72	0.76	0.78	0.75	0.74	0.80	0.76	0.68	0.79
Al_2O_3	16.33	16.58	15.31	20.35	20.33	19.58	19.81	20.54	17.82	20.09
Fe_2O_3T	11.83	17.25	11.45	14.82	15.74	13.97	10.33	9.38	11.21	10.09
MnO	0.16	0.26	0.25	0.32	0.34	0.27	0.50	1.48	0.52	0.44
MgO	1.71	4.04	4.61	5.49	5.65	5.45	3.92	4.43	5.50	3.36
CaO	4.34	2.44	2.94	0.58	0.59	0.56	1.98	3.26	3.27	2.52
Na_2O	0.84	1.08	1.46	2.02	1.99	2.11	5.30	4.42	4.56	5.15
K_2O	7.06	5.77	5.20	5.90	5.88	5.35	3.48	3.57	3.68	3.71
P_2O_5	0.15	0.15	0.17	0.15	0.16	0.15	0.19	0.16	0.17	0.19
LOI	5.18	4.8	4.87	4.81	4.79	4.96	3.53	3.93	4.72	3.8
K	58594	47896	43180	48934	48751	44357	28917	29642	30524	30823
Sc	31.4	32	29.8	29.49	27.86	27.98	27.55	29.44	33.4	28.47
Ti	3686	3781	4162	4458	4292	4242	4591	4414	3954	4723
V	219	230	219	241	231	237	183	247	250	192
Cr	131	140	119.9	57.91	43.35	55.37	14.78	34.9	83.23	32.03
Mn	1134	1977	1949	2391	2430	2106	3782	10760	3939	3443
Co	26.1	23.9	26.0	35.52	36.54	32.57	22.83	24.98	27.82	23
Ni	27.5	38.1	35.2	18.22	17.49	23.19	6.841	13.74	31.98	10.51
Cu	27.1	10.1	16.8	57.6	15.99	15.95	32.01	53.94	11.65	40.39
Zn	32.6	58	54.4	95.57	97.39	85.81	160.4	376.8	170.2	352.4
Ga	14.8	14.2	14.7	18.23	18.06	17.56	18.59	19.36	14.09	19.65
Ge	1.65	1.68	1.91	1.568	1.531	1.404	1.466	1.639	1.603	1.585
Rb	287	218	175	231	214	214	114	127	107.5	129.5
Sr	41.2	53.1	49.0	77.46	71.33	82.51	200	344.8	117.2	212.8
Y	11.8	12.5	22.4	15.09	14.24	14.83	19.72	16.76	15.79	19.8
Zr	45.1	46.2	131.6	59.7	56.2	56.7	47.3	58.4	48.4	48.0
Nb	1.61	1.71	4.02	2.32	2.33	2.27	1.87	2.33	1.82	1.91
Cs	6.1	5.11	2.09	5.36	4.89	6.17	2.25	2.71	0.59	2.42
Ba	1410	1518	1164	1821	1706	1501	1408	2138	1117	1185
La	4.41	3.54	5.79	2.30	2.05	6.30	5.48	7.46	11.52	5.05
Ce	9.79	8.39	16.0	5.99	5.39	14.5	13.3	17.3	24.9	13.0
Pr	1.47	1.26	2.78	0.94	0.86	1.97	2.08	2.37	3.21	2.04
Nd	6.68	5.79	13.3	4.76	4.24	8.59	10.2	10.3	14.4	10.1
Sm	1.95	1.76	4.05	1.53	1.43	1.93	2.77	2.55	3.32	2.80
Eu	0.69	0.46	1.30	0.56	0.52	0.57	1.07	0.99	1.27	1.08
Gd	2.21	2.11	3.90	1.87	1.75	2.09	3.05	2.83	3.33	3.07
Tb	0.39	0.37	0.73	0.38	0.36	0.38	0.55	0.49	0.54	0.55
Dy	2.33	2.34	4.20	2.55	2.40	2.47	3.46	3.05	3.07	3.54
Ho	0.48	0.52	0.86	0.60	0.56	0.57	0.77	0.67	0.62	0.76
Er	1.36	1.48	2.31	1.78	1.68	1.71	2.16	1.89	1.66	2.12
Tm	0.19	0.21	0.34	0.27	0.26	0.26	0.32	0.28	0.24	0.32
Yb	1.26	1.44	2.17	1.83	1.69	1.70	2.09	1.83	1.57	2.09
Lu	0.2	0.22	0.35	0.30	0.28	0.28	0.34	0.30	0.24	0.34
Hf	1.45	1.52	3.41	1.69	1.60	1.58	1.40	1.68	1.34	1.44
Ta	0.13	0.13	0.32	0.18	0.18	0.17	0.13	0.18	0.13	0.14
Pb	2.68	2.8	2.97	3.39	1.71	3.29	3.19	5.00	8.50	3.52
Th	1.87	1.91	6.63	1.45	1.38	1.41	0.77	1.45	1.50	0.77
U	0.56	0.54	1.94	0.44	0.43	0.41	0.25	0.45	0.37	0.24
Mg#	25	35	48	46	46	48	47	52	53	44
$K_2O + Na_2O$	7.90	6.86	6.66	7.91	7.86	7.45	8.78	7.99	8.24	8.86
K_2O/Na_2O	8.46	5.32	3.57	2.93	2.96	2.54	0.66	0.81	0.81	0.72
La/Sm	2.26	2.01	1.43	1.50	1.43	3.26	1.98	2.92	3.47	1.80
Ba/Th	754	795	176	1253	1234	1062	1824	1473	745	1533
La/Yb	3.50	2.46	2.67	1.26	1.22	3.70	2.62	4.07	7.33	2.42

Major element oxide contents are normalized to 100 wt.% on a volatile-free basis. $Mg^{\#}$ (Mg-number) = molar $Mg \times 100/(Mg + Fe^{2+})$, calculated assuming $FeO/(FeO + Fe_2O_3) = 0.85$. Fe_2O_3T = total Fe is given as Fe_2O_3. LOI = Loss on ignition. The normalization factor for the calculation is from Sun and McDonough (1989).

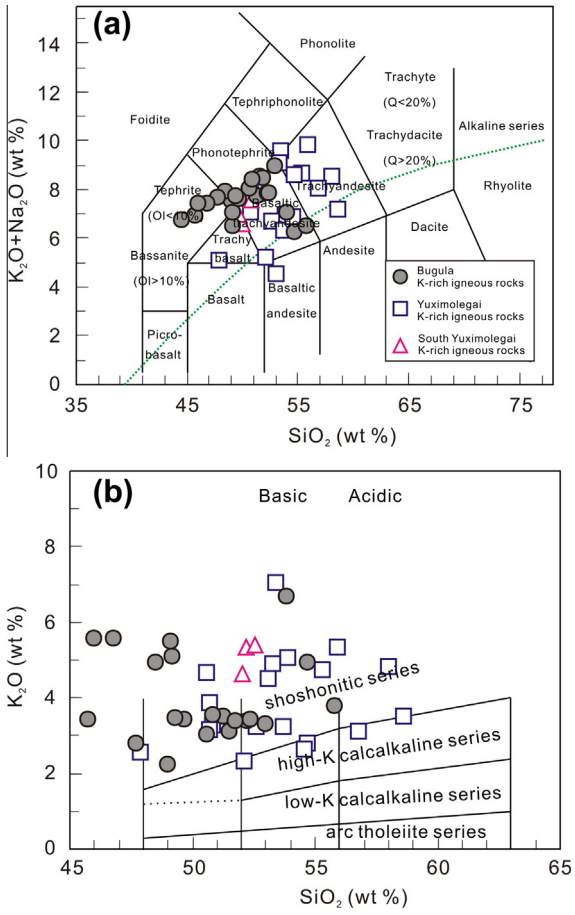

Fig. 3. (a) Total alkali silica and (b) K_2O versus SiO_2 classification diagrams for the Late Paleozoic K-rich igneous rocks from the Awulale Mountains, western Chinese Tianshan. Classification boundaries are from Lebas et al. (1986). The data for Yuximolegai and South Yuximolegai K-rich igneous rocks are from Yang et al. (2012) and Sun et al. (2008), respectively.

4.2. Trace elements of primary carbonates

The globular carbonates hosted in the Bugula K-rich igneous rocks have 57.3–62.5 wt.% CaO, 0–0.7 wt.% SiO_2, 0.1–0.8 wt.% FeO_{tot} and 0.0–0.6 wt.% MgO, indicating they are calcio-carbonates. They have low concentrations of LILEs, with 0.08–0.14 ppm Rb, 1.36–4.25 ppm Ba and 0.34–0.60 ppm Pb (Table 2), compared to the host Bugula K-rich igneous rocks. They are characterized by low REE abundances, with total REE ranging from 34 to 140 ppm. Chondrite-normalized REE patterns (Fig. 6b) and primitive mantle-normalized incompatible element diagrams (Fig. 6d) show the carbonate globules have slightly enriched LREE and relatively flat HREE profiles, with chondrite-normalized La/Yb and Dy/Yb ratios of 6–5 and 0.8–1.7, respectively. Depletion of Ti in the mantle-normalized incompatible trace element patterns (Fig. 6d) indicates that Ti is very incompatible in the primary calcio-carbonate magma.

4.3. Sr, Nd and Pb isotopic systematics

Measured and calculated initial (300 Ma) Sr, Nd and Pb isotopic compositions of selected K-rich igneous rock samples are presented in Tables 3 and 4. The samples are characterized by a limited range of initial isotope ratios with no correlation with rock type. The K-rich igneous rocks from Bugula have elevated radiogenic $^{87}Sr/^{86}Sr_i$ (0.705437–0.705853) and low $^{143}Nd/^{144}Nd_i$ (0.512392–0.512490) relative to Bulk Earth (Table 3), and elevated $^{207}Pb/^{204}Pb_i$ (15.539–15.587) and $^{208}Pb/^{204}Pb_i$ (37.771–38.746) at a given $^{206}Pb/^{204}Pb_i$ (17.912–18.824) compared to the Northern Hemisphere Reference Line (NHRL; Hart, 1984) (Table 4). Similarly, the K-rich igneous rocks from Yuximolegai have similar Sr–Nd isotopes to the K-rich igneous rocks from Bugula (Table 3), and also have relatively high $^{207}Pb/^{204}Pb_i$ (15.558–15.574) and $^{208}Pb/^{204}Pb_i$ (37.956–38.303) at a given $^{206}Pb/^{204}Pb_i$ (18.074–18.310) (Table 4, Fig. 7). In Fig. 7, the Sr–Nd–Pb isotopic compositions of global subducting sediment (GLOSS; Plank and Langmuir, 1998) and some previously published data for K-rich igneous rocks from the Awulale Mountains (Sun et al., 2008; Yang et al., 2012) are shown for comparison. The initial ratios of Sr isotope for K-rich igneous rocks from the Awulale Mountains are significantly lower than those of GLOSS (0.71730; Plank and Langmuir, 1998), while the initial Pb isotopes ratios are close to the field of GLOSS (Fig. 7).

4.4. Carbon and oxygen isotopes of carbonates

The C–O isotope compositions of the calcio-carbonate globules hosted in the Bugula K-rich igneous rocks and the calcite veins associated with Cu-mineralization in Yuximolegai, Chagangnuoer and Wulangdaban from the Awulale Mountains are presented in Table 5 and illustrated in Fig. 8. $\delta^{13}C_{V\text{-}PDB}$ and $\delta^{18}O_{V\text{-}SMOW}$ of seven Bugula calcio-carbonate samples vary from −0.9‰ to −1.2‰ and from 11.7‰ to 16.3‰, with average $\delta^{13}C_{V\text{-}PDB}$ and $\delta^{18}O_{V\text{-}SMOW}$ values being 0.3‰ and 13.4‰, respectively (Table 5). The calcite veins associated with Cu-mineralization from the Awulale Mountains have $\delta^{13}C_{V\text{-}PDB}$ and $\delta^{18}O_{V\text{-}SMOW}$ varying from −3.5‰ to 0.2‰ and from 8.0 to 11.0, respectively (Table 5). In the $\delta^{18}O$ versus $\delta^{13}C$ diagram (Fig. 8), most of the globular calcio-carbonate and calcite veins lie within the field for European and American carbonatites, between the field of primary carbonatites (Taylor et al., 1967) and limestone (Bell and Simonetti, 2010).

5. DISCUSSION

5.1. Origin of carbonate globules

The petrological textures, mineralogy and geochemistry of the calcio-carbonates in the Bugula K-rich igneous rocks are consistent with them being of a primary magmatic origin. The occurrence of calcio-carbonates with spherical or ellipsoidal textures suggests that carbonate melts aggregated before the complete consolidation of the parental silicate melt. Furthermore, some are deformed ovals, indicated flow and deformation in a not fully solidified state. This is also indicated by the isolated distribution of both carbonate and silicate melt inclusions in the globular calcite, which are of primary origin as Guzmics et al. (2012) reported from the Kerimasi volcano (Tanzania).

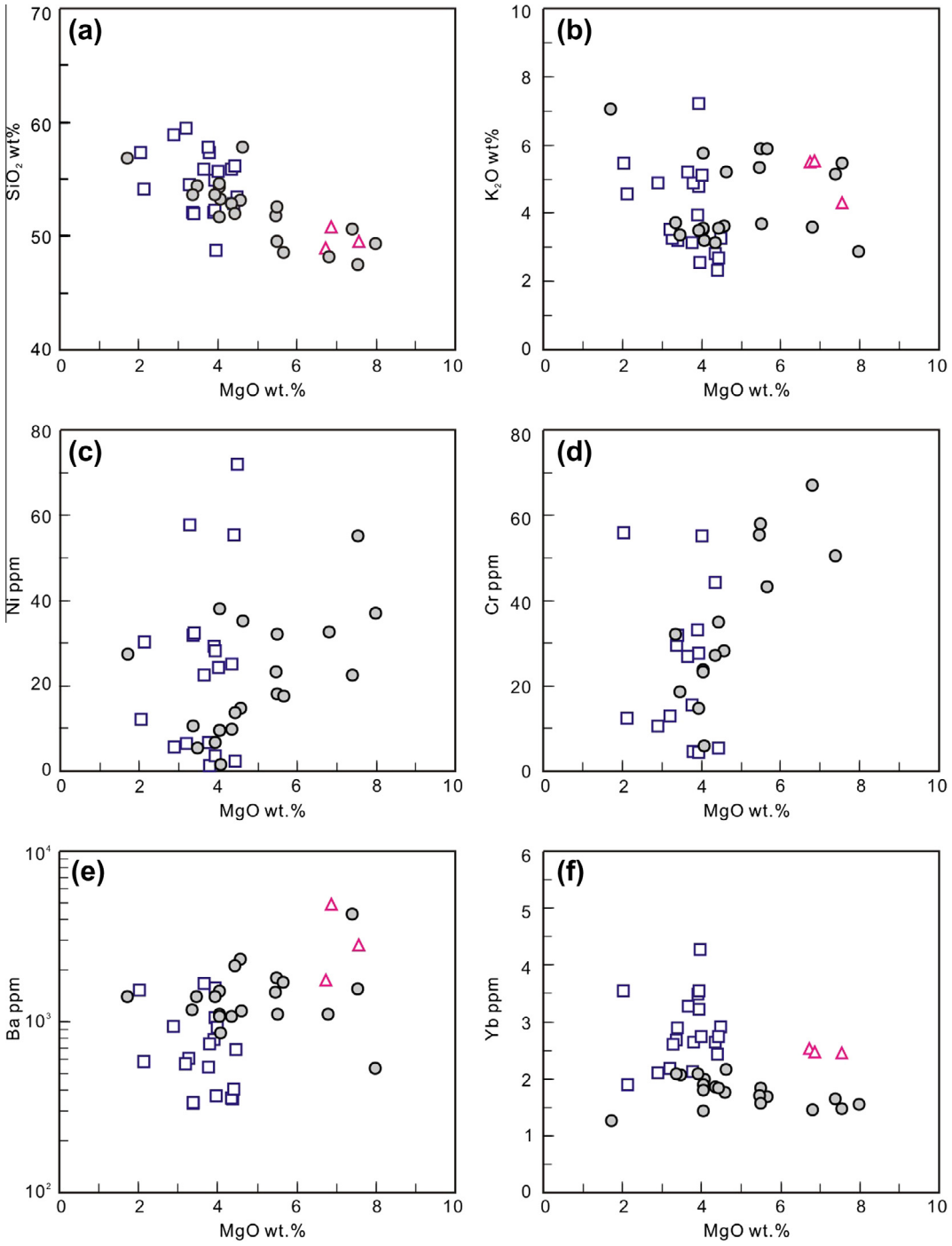

Fig. 4. Selected major element oxide (wt.%) and trace element (ppm) concentrations versus MgO content (wt.%) illustrating the broad compositional range of the K-rich igneous rocks in the Awulale Mountains. All the major element data have been recalculated to 100 wt.% on a volatile-free basis. Data sources and symbols as in Fig. 3a.

There are three probable mechanisms for the formation of primary carbonate magma, including: (1) direct melting of carbonated mantle components (Wallace and Green, 1988; Yaxley et al., 1991), (2) separation of an immiscible carbonate melt from an initially homogeneous CO_2-rich alkaline silicate magma by carbonate–silicate liquid immiscibility (Hamilton et al., 1979; Kogarko et al., 1995; Stoppa et al., 2005; Brooker and Kjarsgaard, 2011), and (3) extensive fractional crystallization of a carbonate-bearing or CO_2-rich alkaline silicate magma (Watkinson and Wyllie, 1971; Dasgupta et al., 2007; Zeng et al., 2010; de Ignacio et al., 2012). Petrological and geochemical studies suggest that the last two processes are likely responsible for the formation of the carbonate globules.

Carbonates hosted in Bugula K-rich igneous rock are calcio-carbonates with low SiO_2 (<1 wt.%) and MgO

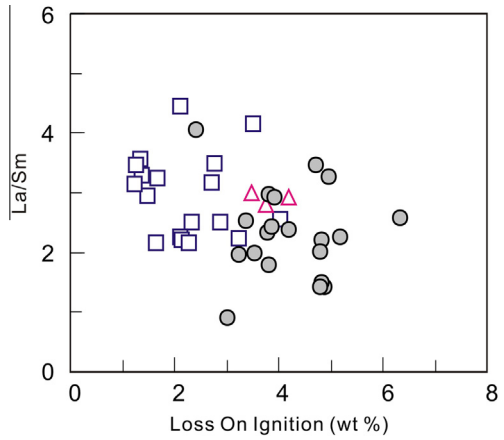

Fig. 5. La/Sm versus loss on ignition for the K-rich igneous rocks from the Awulale Mountains, western Chinese Tianshan. Data sources and symbols as in Fig. 3a.

(<1 wt.%) contents and low concentrations of compatible elements (such as Cr and Ni) (Table 3), which should be relatively enriched in melts in equilibrium with carbonate-rich peridotite, suggesting they did not form by direct melting of the mantle. For comparison, extrusive Mg-carbonatites (lapilli) from Tamazert in Morocco, which were interpreted to have formed from a direct partial melt of the mantle, have consistently higher MgO contents (16–18 wt.%) and 650–2120 ppm Cr (Mourtada et al., 1997).

The petrological textures and geochemistry of the Bugula carbonates are consistent with formation by liquid immiscibility. Both Pyle and Haggerty (1994) and Kogarko et al. (1995) interpreted globular calcite crystals in mantle xenoliths as products of liquid immiscibility under upper mantle conditions. The immiscible carbonate melts usually have high LREE/HREE ratios (Kogarko et al., 1995; de Ignacio et al., 2012). This is seen in multi-element diagrams for the Bugula carbonate, which compare the host K-rich igneous rocks (Fig. 6b) with carbonate globules (Fig. 6d). In the Hamilton projection (Hamilton et al., 1979), the compositions of K-rich igneous rocks plot at the boundary of the two-liquid field, whereas the carbonates plot inside the field of a single carbonate liquid (Fig. 9), suggesting that they are generated from separation of a parental magma. In addition, the co-existence of high temperature silicate- and carbonate-melt inclusions in the calcite globules provides petrological evidence for carbonate–silicate liquid immiscibility (Sokolov, 2002; Guzmics et al., 2012; Solovova and Girnis, 2012). According to their respective partition coefficients, many elements will preferentially partition into one of the conjugate liquids when parental carbonated silicate magma undergoes carbonate–silicate liquid immiscibility. Experimental constraints on the carbonate/silicate liquid–liquid distribution coefficients suggest that rare metals such as Nb, Zr, REE, Th and U concentrate in silicate liquids (Veksler et al., 1998, 2012). Therefore carbonate melt that carry extremely

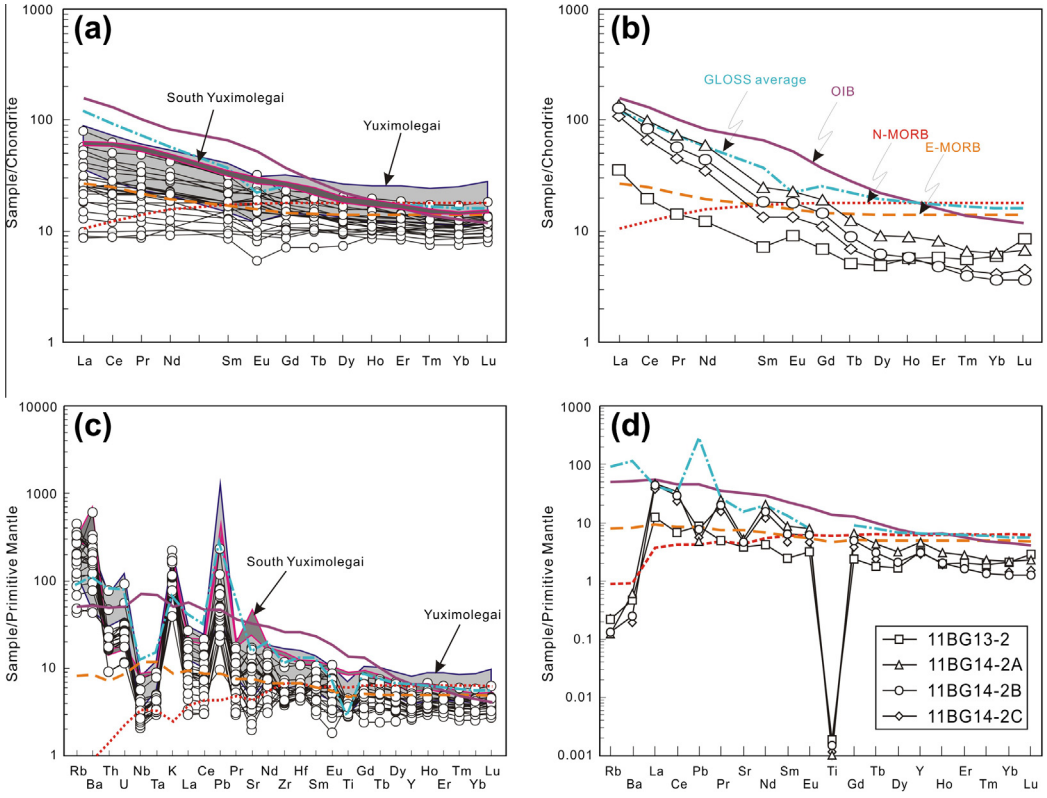

Fig. 6. REE distribution patterns (a and b) and trace element spider diagrams (c and d) for the Bugula K-rich igneous rocks and the primary carbonate globules from the Awulale Mountains, western Chinese Tianshan. The primary mantle and chondrite normalized data, and OIB, N-MORB and E-MORB data are from Sun and McDonough (1989).

Table 2
Major element (wt.%, by EMPA) and trace element compositions (ppm, by ICPMS) of the representative globular calico-carbonate in the Bugula K-rich igneous rocks from Awulale Mountains. Note that, bdl means below detection limit.

Samples	BG8-17d5	BG-9a3	BG8-3-3a	Samples	11BG-13	11BG14-2A	11BG14-2B	11BG14-2C
SiO_2	bdl	bdl	0.65	Sc	5.90	6.39	6.00	4.51
TiO_2	bdl	bdl	0.08	Ti	2.43	1.33	1.97	1.52
Al_2O_3	0.02	bdl	0.69	V	1.50	1.04	0.90	0.35
FeO	0.21	0.09	0.80	Cr	1.35	1.29	1.77	0.80
MnO	0.45	0.41	0.85	Mn	2782	3567	5775	5594
MgO	0.01	0.11	0.56	Co	1.11	1.05	1.19	0.82
CaO	62.53	61.31	57.34	Ni	16.01	14.43	18.21	11.62
Na_2O	0.04	bdl	0.04	Cu	39.28	11.24	56.84	39.76
K_2O	bdl	bdl	0.04	Zn	4.74	2.74	3.78	3.26
P_2O_5	0.02	0.05	0.01	Ga	0.30	0.94	0.87	0.62
Total	63.27	61.97	61.05	Ge	0.06	0.19	0.15	0.14
				Rb	0.14	0.08	0.08	0.14
				Sr	79.43	110.90	96.54	83.07
				Y	14.33	21.12	13.81	12.94
				Ba	3.22	4.25	1.75	1.36
				La	8.36	31.66	29.74	25.35
				Ce	11.85	59.29	50.48	40.26
				Pr	1.33	6.85	5.35	4.21
				Nd	5.68	27.32	20.41	15.95
				Sm	1.09	3.78	2.75	2.02
				Eu	0.53	1.31	1.02	0.77
				Gd	1.41	3.93	2.93	2.23
				Tb	0.19	0.46	0.33	0.26
				Dy	1.23	2.27	1.54	1.35
				Ho	0.32	0.50	0.33	0.31
				Er	0.96	1.33	0.78	0.82
				Tm	0.14	0.17	0.10	0.11
				Yb	1.01	1.06	0.61	0.69
				Lu	0.21	0.17	0.09	0.11
				Pb	0.60	0.34	0.54	0.39

high abundances of rare metals are not likely to have formed by liquid immiscibility (Veksler et al., 2012). However, liquid immiscibility alone cannot account for all of the geochemical differences between the globular carbonates and the K-rich igneous rocks, for example, the relatively low Sr concentrations and the low REE fractionation in the calcio-carbonates.

Evidence of fractional crystallization of a CO_2-rich alkaline parent magma is supported by the mineralogical and geochemical affinities between the globular carbonates and K-rich basaltic rocks. The relatively low Mg abundances (MgO < 8 wt.%) and Mg-numbers ($Mg^{\#} < 64$) of the host mafic alkaline magma indicate that the magmatic source of the K-rich igneous rocks from the Awulale Mountains was not a primitive mantle melt, but rather had undergone differentiation (e.g., Luhr et al., 1995). Early crystallization of olivine and clinopyroxene would strongly deplete the remaining melt in compatible elements, such as Ni, Co, Cr, Fe_2O_3T and MgO (Fig. 4). The crystallization of Fe–Ti oxides would strongly deplete Ti and V in the residual magma, accounting for the negative titanium anomalies in the carbonates (Fig. 6d). Later fractionation of alkali feldspar could also explain the Sr and alkali (K & Na) depletion in the carbonates. Thus, we interpret these carbonate globules as cumulates of a fractionated immiscible carbonate melt, which was derived from liquid immiscibility of a carbon- and K-rich parental magma. If the immiscible carbonate melt separates completely, it could accumulate to form isolated veins of carbonate or calcite because of its relatively low density.

5.2. Source of the carbon- and K-rich alkaline magma

5.2.1. Mantle wedge metasomatism

Mantle metasomatism and partial melting are important geological processes in the deep Earth, whereas partial melting of subducted crustal components is the most important agent for generating mantle metasomatism (Zhang, 2005; Sun et al., 2013). Carbonate melts from the melting of subducted sediments will interact with surrounding peridotite to carbonate the mantle (Rudnick et al., 1993; Tilton et al., 1998; Dasgupta et al., 2009). Many studies have documented that the metasomatism of mantle wedges above the subducting slab is predominantly constrained by two different processes, namely melting and devolatization (decarbonation and dehydration) of the subducted slab (e.g., Turner and Hawkesworth, 1997; Gorman et al., 2006; Poli et al., 2009; Marin-Ceron et al., 2010; Labanieh et al., 2012). The chemical compositions of the K-rich igneous rocks from the Awulale Montains presented

Table 3
Sr and Nd isotopic compositions of the K-rich igneous rocks in Awulale Mountains.

Sample	$^{87}Rb/^{86}Sr$	$^{87}Sr/^{86}Sr$	2σ	$(^{87}Sr/^{86}Sr)_i$	$\varepsilon_{Sr}(t)$	$^{147}Sm/^{144}Nd$	$^{143}Nd/^{144}Nd$	2σ	$(^{143}Nd/^{144}Nd)_i$	$\varepsilon_{Nd}(t)$	$T_{DM,2}$ (Ma)
Bugula											
BG7-2K	11.9526	0.756464	0.000005	0.705437	18.3	0.1833	0.512831	0.000007	0.512471	4.28	713
BG-9	1.9247	0.713734	0.000004	0.705517	19.4	0.1723	0.512827	0.000008	0.512489	4.63	684
BG08-2A	1.2409	0.711020	0.000005	0.705723	22.3	0.1983	0.512845	0.000011	0.512456	3.99	737
BG08-7	0.7987	0.709263	0.000005	0.705853	24.2	0.1438	0.512674	0.000009	0.512392	2.73	839
BG08-8B	0.9537	0.709784	0.000005	0.705713	22.2	0.1365	0.512759	0.000007	0.512490	4.66	682
BG08-9	0.5686	0.708027	0.000006	0.705600	20.6	0.1528	0.512713	0.000012	0.512413	3.14	806
BG08-17	0.9000	0.709378	0.000006	0.705536	19.7	0.1576	0.512729	0.000012	0.512420	3.28	794
BG'08-2-4	0.9699	0.709662	0.000005	0.705522	19.5	0.1359	0.512682	0.000006	0.512415	3.20	801
BG'08-3-4	2.2356	0.715075	0.000004	0.705531	19.6	0.2886	0.512974	0.000010	0.512407	3.03	815
Yuximolegai											
YXAn-8	0.4642	0.706846	0.000005	0.704864	10.1	0.1496	0.512728	0.000008	0.512434	3.56	772
YX2-2	0.2799	0.705887	0.000017	0.704692	7.7	0.1427	0.512804	0.000008	0.512524	5.31	629
YX2-7	0.7651	0.707140	0.000017	0.703874	−3.9	0.1447	0.512782	0.000009	0.512498	4.80	670
YX3-3	0.4078	0.705920	0.000007	0.704179	0.4	0.1362	0.512794	0.000007	0.512527	5.37	624
YX2-1	0.8413	0.708568	0.000018	0.704976	11.7	0.1342	0.512763	0.000009	0.512499	4.84	668
YX2-5	1.0428	0.709631	0.000017	0.705179	14.6	0.1411	0.512786	0.000009	0.512509	5.02	653
YX2-6	0.9821	0.708508	0.000014	0.704315	2.3	0.1361	0.512791	0.000008	0.512524	5.31	629
South Yuximolegai											
04XJ-282	0.5825	0.707720	\	0.705233	15.4	0.1400	0.512727	\	0.512452	3.91	743

Note: Chondritic uniform reservoir (CHUR) at the present day [$(^{87}Rb/^{86}Sr)_{CHUR} = 0.0847$ (McCulloch and Black, 1984); $(^{87}Sr/^{86}Sr)_{CHUR} = 0.7045$ (DePaolo, 1988); $(^{147}Sm/^{144}Nd)_{CHUR} = 0.1967$ (Jacobsen and Wasserburg, 1980); $(^{143}Nd/^{144}Nd)_{CHUR} = 0.512638$ (Goldstein et al., 1984)] was used for the calculations of the initial epsilon Sr–Nd values. $\lambda_{Rb} = 1.42 \times 10^{-11}$ year^{-1} (Steiger and Jäger, 1977); $\lambda_{Sm} = 6.54 \times 10^{-12}$ year^{-1} (Lugmair and Marti, 1978). Both $\varepsilon_{Nd}(t)$ and $\varepsilon_{Sr}(t)$ were calculated using the age of 300 Ma. Data for samples from Yuximolegai are from Yang et al. (2012) and data for samples from South Yuximolegai are from Sun et al. (2008).

Table 4
Pb isotopic compositions of the K-rich igneous rocks in Awulale Mountains.

	$^{206}Pb/^{204}Pb$	$^{207}Pb/^{204}Pb$	$^{208}Pb/^{204}Pb$	$^{238}U/^{204}Pb$	$^{235}U/^{204}Pb$	$^{232}Th/^{204}Pb$	$(^{206}Pb/^{204}Pb)_i$	$(^{207}Pb/^{204}Pb)_i$	$(^{208}Pb/^{204}Pb)_i$	Δ7/4	Δ8/4
Bugula											
BG7-1K	19.474	15.621	39.468	13.645	0.099	47.081	18.824	15.587	38.764	5.5	37.9
BG-9	18.644	15.579	38.452	13.698	0.099	44.297	17.991	15.545	37.790	10.4	41.1
BG-8	18.601	15.575	38.484	14.456	0.105	47.695	17.912	15.539	37.771	10.6	48.8
Yuximolegai											
YX-An4	18.517	15.585	38.524	4.353	0.032	14.750	18.310	15.574	38.303	9.8	54.0
YX2-2	18.688	15.59	38.795	12.844	0.093	56.140	18.076	15.558	37.956	10.8	47.4
YX2-7	18.751	15.602	38.887	14.219	0.103	58.890	18.074	15.567	38.006	11.6	52.8
YX2-1	18.679	15.587	38.745	11.263	0.082	48.474	18.142	15.559	38.020	10.1	45.9
YX2-5	19.021	15.612	39.017	19.290	0.140	68.904	18.102	15.564	37.987	11.1	47.4
YX2-6	18.627	15.591	38.711	10.247	0.074	44.656	18.139	15.565	38.043	10.8	48.6

Note: $\lambda_{U238} = 0.155125 \times 10^{-9}$ year^{-1}, $\lambda_{U235} = 0.98485 \times 10^{-9}$ year^{-1} and $\lambda_{Th232} = 0.049475 \times 10^{-9}$ year^{-1} (Steiger and Jäger, 1977). $(^{207}Pb/^{204}Pb)_{NHRL} = 0.1084 \times (^{206}Pb/^{204}Pb)_i + 13.491$; $(^{208}Pb/^{204}Pb)_{NHRL} = 1.209 \times (^{206}Pb/^{204}Pb)_i + 15.627$ (Hart, 1984). Initial Pb isotope ratios were obtained by using the age of 300 Ma.

here are consistent with a mantle source affected by slab decarbonation and dehydration rather than melting of subducted sediments.

Dehydration and decarbonation of slab sediments will occur before melting due to their *P–T* profiles (Syracuse and Abers, 2006; Syracuse et al., 2010), and the resulting fluids will play a critical role in the fertilization and melting of the mantle wedge (Kogiso et al., 1997; Gorman et al., 2006; Zhang et al., 2007). The relative immobility of some incompatible elements (e.g., Th, HFSE) in aqueous fluids has long been used to distinguish between the roles of melts and fluids as metasomatising agents (Labanieh et al., 2012). The Th budget in arc-related volcanic rocks is usually considered to be controlled by sediment recycling (Plank and Langmuir, 1998). High Th concentrations, Th/Nb, and La/Sm ratios in subduction-related lavas have been interpreted to have been caused by the incorporation of recycled sediments (Avanzinelli et al., 2009; Labanieh et al., 2012). Conversely, subduction-related fluids are generally considered enriched in elements such as Ba, Pb, Rb, U and Sr and depleted in Th, Nb, Ta, Hf, Ti and REE (Brenan et al., 1995; Ayers et al., 1997; Elliott et al., 1997; Kessel

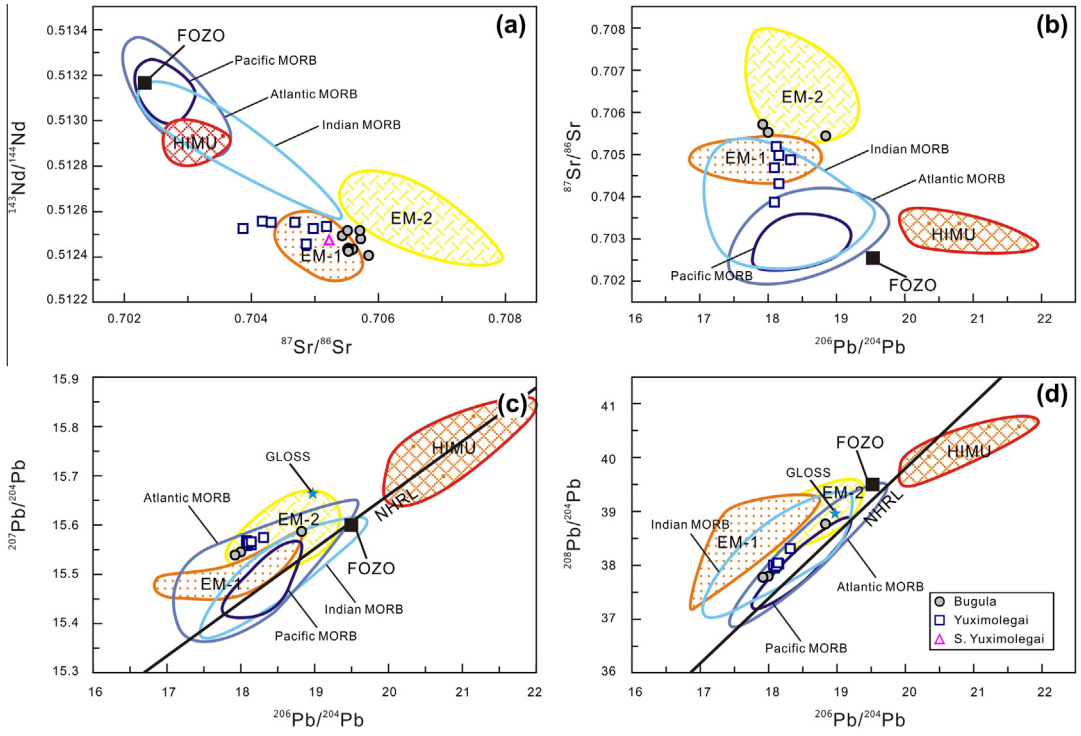

Fig. 7. Sr–Nd–Pb isotopic compositions of the K-rich igneous rocks in the Awulale Mountains. MORB, OIB, FOZO, HIMU, EM1 and EM2 data from Hofmann (1997). The average isotopic compositions of GLOSS are from Plank and Langmuir (1998), with $^{87}Sr/^{86}Sr = 0.71730$, $^{143}Nd/^{144}Nd = 0.51218$, $^{206}Pb/^{204}Pb = 18.913$, $^{207}Pb/^{204}Pb = 15.673$ and $^{208}Pb/^{204}Pb = 38.899$.

et al., 2005), which are consistent with the trace elements distribution patterns for the K-rich igneous rocks in the Awulale Mountains (Fig. 6c). Labanieh et al. (2012) attributed the high Ba/Th and $^{143}Nd/^{144}Nd$ ratios and low La/Sm and $^{87}Sr/^{86}Sr$ ratios in arc lavas on Martinique to the influence of aqueous fluids formed by slab dehydration, whereas, they attributed the lavas with low Ba/Th and $^{143}Nd/^{144}Nd$ ratios and high La/Sm and $^{87}Sr/^{86}Sr$ ratios to the influence of hydrous melts by melting of slab sediments. In the Awulale Moutains, the K-rich igneous rocks are characterized by high Ba/Th ratios and low $^{87}Sr/^{86}Sr$ and La/Sm ratios (Figs. 7 and 10), suggesting that they are predominately influenced by slab dehydration rather than melting of sediments. In contrast, the Late Paleozoic igneous rocks in western Chinese Tianshan show a combination of both dehydration and melting (Fig. 10).

The depth and geothermal gradient of the subducted slab are the dominant factor controlling whether slab dehydration or melting will occur. Sediment melting can only occur when the subducted slab reaches sufficiently high pressure and temperature conditions and will generally occur at greater depths than slab dehydration (Thomsen and Schmidt, 2008; Labanieh et al., 2012). Experimental studies of Thomsen and Schmidt (2008) demonstrate that carbonate-saturated pelites (e.g., marls) produce potassic melts at temperatures from 900 °C to 1070 °C and at pressures from 2.5 GPa to 5.0 GPa. When mixed with depleted mantle wedge, these melts can serve as suitable metasomatic agents for K-rich magmatism (Avanzinelli et al., 2009). However, the K-rich igneous rocks in the Awulale Mountains are characterized by the geochemical features of a spinel lherzolite mantle source, with pressure less than 2.5 GPa (<80 km depth).

5.2.2. Partial melting of the metasomatized mantle wedge

K-rich igneous rocks, both potassic and ultra-potassic, are usually considered to have formed from the partial melting of amphibole/phlogopite veins or their host mantle wedge, with their K concentrations controlled by the abundance of amphibole/phlogopite in the vein network, the amounts of mantle component involved, and the degree of partial melting (e.g., Conceição and Green, 2004; Avanzinelli et al., 2009; Conticelli et al., 2009a,b). Effective melting of these vein networks required a slab window setting, induced by the break-off of a subducted slab, for the generation of the K-rich mafic magma in the western Tianshan (Yang et al., 2012).

Amphiboles from mantle xenoliths display relatively high abundances of K, Sr, LREE, HFSE, and, in some cases, Ba, but very low abundances of Rb and Th (Ionov and Hofmann, 1995; Chazot et al., 1996). In contrast, phlogopites are rich in K, Sr, Ba, and Rb, but have very low concentrations of REE, HFSE and Th. The K/Rb ratios of phlogopites vary from 40 to 400, whereas those of amphiboles and amphibole-bearing melt are generally greater than 1100 (Hart and Aldrich, 1967; Chakrabarti et al., 2009). The K-rich igneous rocks in the Awulale Mountains have relatively low K/Rb ratios (154–548), as well as low REE and HFSE abundances, indicating that phlogopites are the dominant hydrous minerals in the source region.

Table 5
C and O isotopic compositions of the calico-carbonate associated with K-rich igneous rocks in Awulale Mountains. $\delta^{18}O_{V\text{-}SMOW}$ (‰) = 1.03091 × $\delta^{18}O_{V\text{-}PDB}$ (‰) + 30.91, according to Coplen et al. (1983).

Sample ID	$\delta^{13}C_{V\text{-}PDB}$ (‰)	$\delta^{18}O_{V\text{-}PDB}$ (‰)	$\delta^{18}O_{V\text{-}SMOW}$ (‰)
Bugula			
BG7-1K	0.6	−16.8	13.6
BG7-2K	−0.9	−18.7	11.7
BG-8	−0.2	−14.2	16.3
BG08-10	1.2	−16.3	14.1
11BG14-2B	−0.1	−17.0	13.3
11BG14-2A	0.4	−17.7	12.7
11BG13	1.0	−18.3	12.1
Yuximolegai			
YX-3K1	−0.9	−21.8	8.5
YX-3K8	−1.1	−21.4	8.8
YX-3K11	−1.6	−21.2	9.1
YX-3K13	−1.2	−21.5	8.8
YXBT7-3C	−1.0	−21.2	9.1
YX7-2	−1.1	−20.7	9.6
YX7-4	−0.7	−19.4	10.9
Chagangnuoer			
CG08-1	−0.3	−20.5	9.8
11CG15-6	−2.4	−21.5	8.8
11CG10-5B	−1.2	−19.3	11.0
11CG15D	−0.4	−20.2	10.1
11CG15A	−0.7	−20.6	9.6
11CG15C	−0.5	−20.6	9.6
PD16	−0.7	−21.1	9.2
PD16-1	0.2	−20.7	9.6
PD16-2-4	−0.8	−21.6	8.6
PD16-2-8	0.1	−21.2	9.1
Wulangdaban			
09WLC-1	−3.0	−21.2	9.0
09WLC-2	−3.3	−21.7	8.5
09WLC-3	−3.2	−22.3	8.0
09WLC-4	−3.5	−22.1	8.1
09WLC-5	−3.3	−22.1	8.1

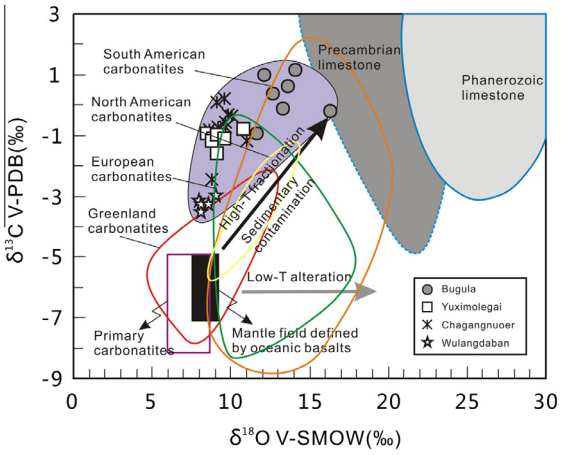

Fig. 8. Oxygen and carbon isotope compositions of calcio-carbonate from Bugula, Yuximolegai, Chagangnuoer and Wulangdaban in the Awulale Mountains (Fig. 1b), compared with the values of carbonatites and limstones (after Bell and Simonetti, 2010). The open box for primary carbonatites with mantle-type oxygen and carbon isotopic compositions are from Taylor et al. (1967), and the solid box for the mantle field defined by oceanic basalts is from Bell and Simonetti (2010). Arrows indicate possible processes (high temperature fractionation or sedimentary carbonate contamination and low temperature alteration) causing shifts from primary values (Hoernle et al., 2002). The size of the symbols is larger than the analytical uncertainties.

In addition, the K-rich igneous rocks are rich in Ba and Rb, which could have resulted from magma generation in a subduction zone, because Ba and Rb are highly incompatible LILE and can be mobilized during metamorphism and hydrothermal alteration induced by subduction (Arculus, 1994; Polat and Hofmann, 2003; Jenner et al., 2009). The variation of Ba/La and Rb/Yb ratios are positively correlated to K_2O contents in the K-rich igneous rocks, which are different from those of the calc-alkaline igneous rocks in the Awulale Mountains (Yang et al., 2012). These different variation trends are consistent with the former being products of melting of phlogopite veins or vein-bearing carbonated mantle wedge, whereas the latter are products of partial melting of a typical mantle wedge (Jenner et al., 2009). Geochemical studies of modern arc-related magmatism have shown that Ba/La can be used as an indicator of the total slab-derived input into the mantle wedge (Carr et al., 1990; Lin et al., 1990; Leeman et al., 1994; Patino et al., 2000; Jenner et al., 2009). Carr et al. (1990) observed that there is a correlation between Ba/La of arc lavas and subduction angle along the Central American arc. They attributed low Ba/La to metasomatism of a larger volume of the overlying mantle wedge during shallow subduction, resulting in a less pronounced subduction signature. The significantly higher Ba/La ratios (17–827) of the K-rich igneous rocks from the Awulale Mountains imply that their generation is associated with a relatively high angle subduction. The Ba/Nb ratio can be taken as an indicator of the amount of fluid in the mantle source region, or as a rough proxy for water content (Cervantes and Wallace, 2003). The Ba/Nb ratios for the K-rich igneous rocks ranging from 73 to 2038, suggest that a considerable amount of hydrous minerals (e.g., phlogopite or amphibole) existed in the source region, and also that only small amounts of mantle components were involved during the vein melting process.

The Dy/Yb ratio is an important geochemical index for distinguishing partial melting between the spinel and garnet stability fields of an amphibole- and/or phlogopite-bearing lherzolite (Duggen et al., 2005; Jiang et al., 2009). Partial melting in the garnet stability field generally leads to high Dy/Yb ratios (>2.5), whereas melting in the spinel stability field would produce melts with low Dy/Yb ratios (<1.5). The K-rich igneous rocks under study have intermediate Dy/Yb ratios ranging from 1.39 to 2.29, which implies that the source mantle contains both garnet-facies and spinel-facies lherzolite. The La/Yb ratios of igneous rocks are sensitive to basalt source mineralogy because Yb is typically more compatible in garnet than in clinopyroxene or spinel (Luhr et al., 1995). The Yb concentrations and La/Yb ratios suggest that the mineral ratios of garnet/spinel in

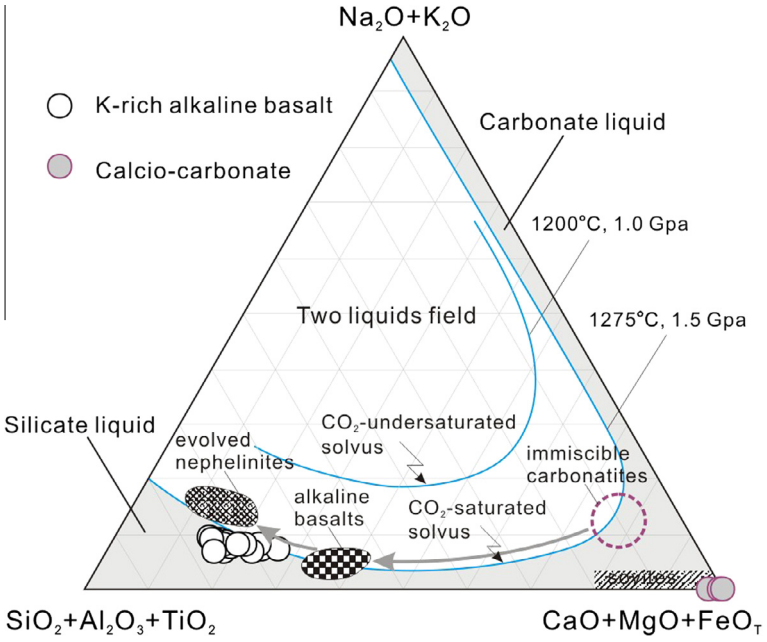

Fig. 9. Hamilton projection (Hamilton et al., 1979) of the calcio-carbonate bearing K-rich igneous rocks from Bugula, illustrating the silicate–carbonate liquid miscibility gaps and a possible melting path of carbonated peridotite (the gray arrow from the area of immiscible carbonatite to alkali basalts to the evolved nephelinites), projected from CO_2 (after Lee and Wyllie, 1997; Tappe et al., 2006)). The 1.0 GPa solvus is from Lee and Wyllie (1997). The 1.5 GPa data is from Brooker (1998).

the source region are all less than 0.25. In the La/Yb versus Yb modal diagram (Fig. 11), all the K-rich igneous rocks plot in the spinel lherzolite field with little evidence of a garnet signature. Consequently the magma source of the Bugula K-rich igneous rocks could be produced by partial melting of 10–25% ($F = 0.10$–0.25) of garnet–spinel lherzolite and those from Yuximolegai and South Yuximolegai could be produced by relatively low degrees of partial melting of 8–15% (Fig. 11). Thus, all K-rich igneous rocks from the Awulale Mountains were likely to derive from partial melting of the garnet–spinel lherzolite transitional field (<27 kbar, Klemme and O'Neill, 2000).

5.2.3. The effects of slab-derived CO_2

Previous work has confirmed that volcanic rocks of arc regions have significantly higher CO_2 content than that of mid-ocean regions (Sano and Williams, 1996; Marty and Tolstikhin, 1998), and also that the existence of CO_2 can trigger the melting of mantle wedge and formation of arc melts (Lin et al., 1990; Ducea et al., 2005). In the subducting slab, the primary hosts of CO_2 are the carbonate minerals that are expected to be resistant to metamorphic breakdown during subduction (Connolly, 2005). Nevertheless, the CO_2 emitted from volcanic arcs (e.g., Wallace, 2005) and the CO_2 bearing fluids within eclogite-facies rocks under high-pressure conditions (e.g., (Gao et al., 2007)) are considered to be derived from subducted slab. Effective release of CO_2 is likely to require open-system decarbonation, flushing of carbonate-rich rocks by aqueous fluids (Zack and John, 2007) or dissolution of carbonates into slab melts or supercritical liquids (Frezzotti et al., 2011). The participation of fluids ($CO_2 + H_2O$) derived from the devolatilization of subducting slabs would reduce the peridotite solidus and play critical roles in the fluxing melting of the mantle wedge and global geochemical cycles (Dasgupta et al., 2013; Spandler and Pirard, 2013).

The solubility of CO_2 in silicate melts is controlled by the effects of pressure, temperature and melts composition, and also dramatically influences the physical properties of magmas, such as density, viscosity, vesicularity, and eruptive styles. For example, Lesne et al. (2011) found twice higher CO_2 solubility in alkali basalts compared with mid ocean ridge melts, and Behrens et al. (2009) also found a higher CO_2 capacity in phono-tephritic melt, which they explained as a consequence of high K content. At a given pressure and temperature, Brooker et al. (2001) proposed that the solubility of CO_2 is a strong function of the "non-bridging oxygen" (NBO) content of the melt, expressed as the NBO/T ratio, where T represents tetrahedral network-forming cations. This observed behavior can be modeled by considering melt polymerization and the proportion of NBO/T (Brooker et al., 2001 and references therein), where Si^{4+} and Al^{3+} are tetrahedral cations (network formers) and Mg^{2+}, Ca^{2+}, and Na^{+} ions are network modifiers that generate NBOs (Iacovino et al., 2013 and references therein). It can also be understood by analogy with the complexing of alkali cations in aqueous solution with CO_2 to form stable alkali carbonate precipitates (Iacovino et al., 2013). Magmas with higher alkali contents will be weakly polymerized compared with less alkaline melts because the large ionization potential of their charge-balancing cations create weaker bridging T–O–T bonds. This weaker polymerization of the melt allows for a higher dissolution of CO_2 through the reaction of CO_2

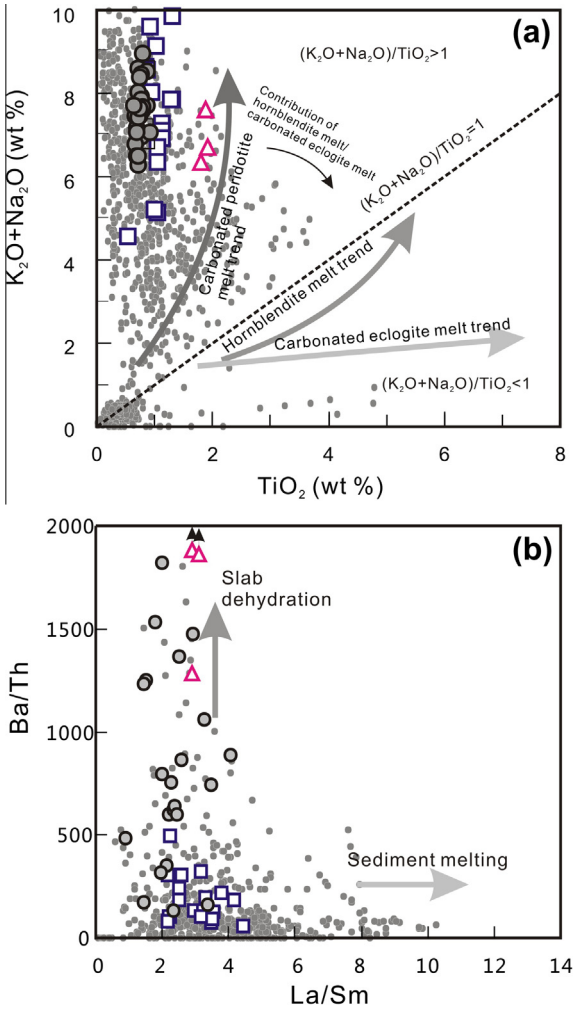

Fig. 10. (a) $K_2O + Na_2O$ versus TiO_2 and (b) Ba/Th versus La/Sm for the K-rich igneous rocks from the Awulale Mountains. The data compilation of gray spots for the Late Paleozoic igneous rocks from western Chinese Tianshan are from Georoc (http://georoc.mpch-mainz.gwdg.de/georoc/). Other data sources and symbols as in Fig. 3a.

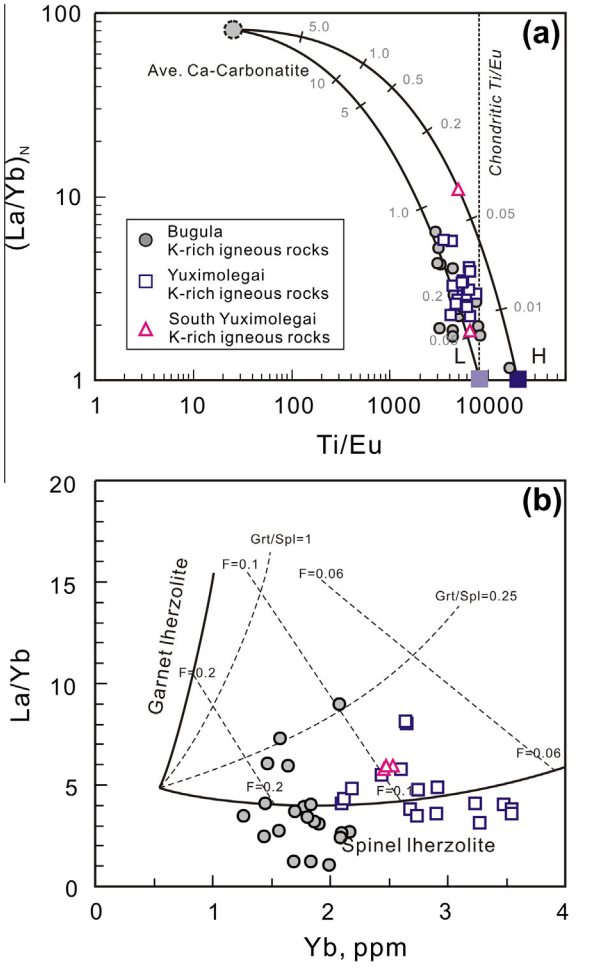

Fig. 11. (a) Ti/Eu versus chondrite-normalized La/Yb ratio for the K-rich igneous rocks from the Awulale Mountains, showing mixing curves between harzburgite (H) and lherzolite (L) (after Rudnick et al., 1993). Numbers adjacent to curves represent percentage of average carbonatite added to peridotites. (b) Yb versus La/Yb plot showing samples of the K-rich igneous rocks in the Awulale Mountains in relation to non-modal partial melting of garnet and spinel lherzolite sources containing different proportions of these minerals (garnet:spinel = 1 or 0.25) following the method of Class et al. (1994). The source is assumed to be enriched relative to chondritic composition (La = 1.79 ppm, Yb = 0.31 ppm). The model of garnet lherzolite is taken as Ol:Opx:Cpx:Grt = 60:25:9:6 and that of the spinel lherzolite as Ol:Opx:Cpx:Sp = 58:30:10:2. Phase proportions entering the melt are taken as Ol:Opx:Cpx:Grt (or Sp) = 10:20:65:5. Partition coefficients for La and Yb were selected from values of Luhr et al. (1995) as 0.0002:0.002:0.069:0.01:0.002 and 0.0015:0.049:0.28:4.1:0.007, for Ol:Opx:Cpx:Grt:Sp.

$(\text{melt}) + 2\text{NBO}^- \leftrightarrow (CO_3)^{2-} + O^0$, where O^0 represents bridging oxygen (Brooker et al., 2001). Therefore, the slab-derived CO_2 plays critical roles in the fluxing melting of the metasomatized mantle wedge and also strongly affects the physical properties of the host magma, thereby influencing arc magma ascent and eruptive behavior.

5.3. Implication for carbon recycling in the subduction zones

Subduction zones modulate the global carbon cycle by transporting carbon into the mantle on the subducting slab and returning carbon back to the surface through arc volcanism (Varekamp et al., 1992; Sano and Williams, 1996). It is estimated that approximately 25% of subducted carbon is lost from the slab through decarbonation processes and the other 75% is carried into the deep mantle (Hofmann, 1997; Sleep and Zahnle, 2001). Carbon isotope compositions show that about 80% of the CO_2 in arc volcanism originates from marine sedimentary carbonates and organic materials by subduction of oceanic crust (Marty and Tolstikhin, 1998). Given that, slab decarbonation at relatively shallow depths and carbonate melting and dissociation in the deep Earth are the three dominate mechanisms for carbon injection into the Earth's mantle. The geochemical characteristics of the K-rich igneous rocks in the Awulale Mountains favor the explanation that there decarbonation of the subducted slab rather than carbonate

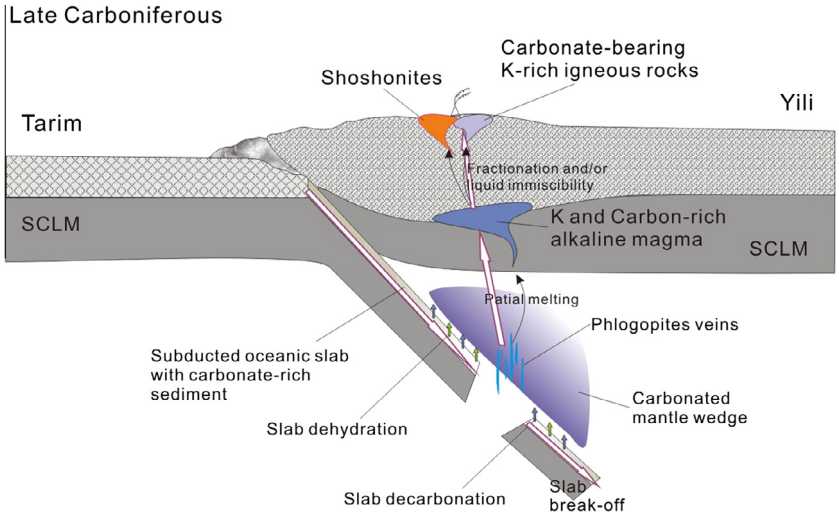

Fig. 12. A model for the primary carbonate-bearing K-rich igneous rocks in the Awulale Mountains, showing the carbon recycling in subduction zones. The mantle wedge is carbonated by the subducted sediment, and subsequently partially melted to generate the carbon- and K-rich alkaline magma in sub-arc region. The primary carbonate and K-rich igneous rocks in Awulale Mountains formed from fractionation during ascent of the CO_2-saturation alkaline magma.

melting or even dissociation was the primary operating mechanism (Fig. 12).

Decarbonation is a metamorphic reaction between silicate and carbonate minerals that releases CO_2, which is considered to be an important mechanism for the global carbon cycle (Gorman et al., 2006). The decarbonation reaction between sediment carbonates and carbonated oceanic crust with high pressure peridotite minerals is critical to metasomatisim of the mantle wedge, and plays an important role in the partial melting of the mantle wedge to generate mafic alkaline melts. These are consistent with the situation of the generation of the parental magma of the K-rich igneous rocks in the Awulale Mountains (Fig. 12). The most important carbonation reaction for peridotites, which changes lherzolite to wehrlite at the mantle pressure proposed by Dalton and Wood (1993), is

$$\underset{Dol}{CaMg(CO_3)_2} + 4\underset{Opx}{MgSiO_3} \rightarrow \underset{Cpx}{CaMgSi_2O_6} + 2\underset{Ol}{Mg_2SiO_4} + 2CO_2 \quad (1)$$

Also, calcio-carbonate can be generated through the reaction of dolomitic carbonate with depleted lherzolite under relatively low pressure through the reactions

$$\underset{Dol}{CaMg(CO_3)_2} + 2\underset{Opx}{MgSiO_3} \rightarrow \underset{Cpx}{CaMgSi_2O_6} + 2\underset{Mgs}{MgCO_3} \quad (2)$$

and

$$\underset{Cpx}{CaMgSi_2O_6} + 3\underset{Mgs}{MgCO_3} \rightarrow \underset{Cal}{CaCO_3} + 2\underset{Ol}{Mg_2SiO_4} + 2CO_2 \quad (3)$$

Consequently, the CO_2 concentration in the mantle would be increased by those decarbonation reactions, and would dissolve into the silicate melts derived from partial melting of the fertilized mantle wedge. Generally, alkali-rich magmas typically have higher CO_2 solubility than their less alkaline counterparts (Behrens et al., 2009; Iacovino et al., 2013). This can be used to explain the transfer mechanisms of carbon and the formation of CO_2-rich parental magma for the carbonate-bearing K-rich igneous rocks (Fig. 12).

In southwestern Tianshan, a huge high-P and low-T metamorphic belt –comprised of mafic metavolcanic rocks, metavolcaniclastic rocks, metagreywacke, marble and serpentinite with a length of at least 200 km and width of over 10 km as so far reported (Gao and Klemd, 2003) – was formed within a Paleozoic accretionary wedge on the south side of the Kazakhstan–Yili plate. The discovery of coesite-bearing schists and eclogites and magnesite dissociation in the metapelites (Zhang et al., 2002a,b; Zhang et al., 2003) indicates that the metapelites experienced ultrahigh-pressure metamorphism with a peak metamorphic age of 320 ± 3.7 Ma and peak metamorphic P–T conditions of 565 °C and 29 kbar (Yang et al., 2013). The peak metamorphic temperature is significantly lower than the solidus temperature of ca. 770 °C at 30 kbar for the carbonated pelitic sediments melting experiment of Tsuno and Dasgupta (2012). The exhumation of large volumes of low-density metapelites also indicates effective melting of the subducted sediments is not the dominate mechanism for liberating carbon in the cold subduction zone of the western Tianshan. Therefore, slab decarbonation, partial melting of carbonated mantle wedge and segregation of CO_2- and K-rich alkaline magma, all played critical roles in the carbon transfer from the subducted sediments into the arc magma in the western Tianshan, and are significant for revealing the carbon recycling mechanisms in the subduction zones.

6. CONCLUSIONS

We conclude that the globular carbonates in the Bugula K-rich igneous rocks are primary and comprised

of calcio-carbonate. The textural and compositional characteristics of the carbonate globules and the host K-rich igneous rocks reported here favor an explanation for the formation by segregation of immiscible carbonate from a differentiated CO_2- and K-rich parental magma. C–O isotopes indicated that the carbon of both of the primary calcio-carbonate and the calcite veins associated Cu (Au)-mineralization in the Awulale Mountains originated from the recycling of subducted oceanic sediments. The K-rich igneous rocks that are widely distributed in the Awulale Mountains, including Bugula, Yuximolegai and South Yuximolegai, were derived from the partial melting of carbonated mantle wedge. Their magma formed by <25% partial melting of phlogopite-bearing garnet–spinel lherzolite. All the K-rich igneous rocks of the Awulale Mountains formed from a mantle source carbonated predominately by slab decarbonation and dehydration rather than the melting of subducted sediments. Therefore, we propose a new important mechanism of carbon-recycling in subduction zones whereby the carbon is released from the subducted slab by decarbonation during subduction and optionally dissolved in alkaline arc magma. By this mechanism the carbon is recycled by K-rich magmatism from the descending slab and into the overlying mantle wedge.

ACKNOWLEDGMENTS

This work was financially supported by the National Natural Science Foundation of China (U1203291, 41173040, 41273056 and 41373031). We appreciate the assistance of Ms. Guangqian Hu and Ying Liu and Mr. Xianglin Tu and Jinlong Ma for determination of elemental and isotopic compositions. We are grateful to Weidong Sun for editorial handling and the three anonymous reviewers for constructive comments that helped improve the manuscript substantially. This is contribution No. IS-1856 from GIGCAS.

REFERENCE

Altherr R., Topuz G., Siebel W., Sen C., Meyer H. P., Satir M. and Lahaye Y. (2008) Geochemical and Sr–Nd–Pb isotopic characteristics of Paleocene plagioleucitites from the Eastern Pontides (NE Turkey). *Lithos* **105**, 149–161.

Arculus R. J. (1994) Aspects of magma genesis in arcs. *Lithos* **33**, 189–208.

Avanzinelli R., Lustrino M., Mattei M., Melluso L. and Conticelli S. (2009) Potassic and ultrapotassic magmatism in the circum-Tyrrhenian region: significance of carbonated pelitic vs. pelitic sediment recycling at destructive plate margins. *Lithos* **113**, 213–227.

Ayers J. C., Dittmer S. K. and Layne G. D. (1997) Partitioning of elements between peridotite and H_2O at 2.0–3.0 GPa and 900–1100 °C, and application to models of subduction zone processes. *Earth Planet. Sci. Lett.* **150**, 381–398.

Bau M. (1991) Rare-earth element mobility during hydrothermal and metamorphic fluid rock interaction and the significance of the oxidation-state of europium. *Chem. Geol.* **93**, 219–230.

Behrens H., Misiti V., Freda C., Vetere F., Botcharnikov R. E. and Scarlato P. (2009) Solubility of H_2O and CO_2 in ultrapotassic melts at 1200 and 1250 °C and pressure from 50 to 500 MPa. *Am. Mineral.* **94**, 105–120.

Bell K. and Simonetti A. (1996) Carbonatite magmatism and plume activity: implications from the Nd, Pb and Sr isotope systematics of Oldoinyo Lengai. *J. Petrol.* **37**, 1321–1339.

Bell K. and Simonetti A. (2010) Source of parental melts to carbonatites-critical isotopic constraints. *Mineral. Petrol.* **98**, 77–89.

Boari E., Avanzinelli R., Melluso L., Giordano G., Mattei M., De Benedetti A. A., Morra V. and Conticelli S. (2009) Isotope geochemistry (Sr–Nd–Pb) and petrogenesis of leucite-bearing volcanic rocks from "Colli Albani" volcano, Roman Magmatic Province, Central Italy: inferences on volcano evolution and magma genesis. *Bull. Volcanol.* **71**, 977–1005.

Brenan J. M., Shaw H. F., Ryerson F. J. and Phinney D. L. (1995) Mineral-aqueous fluid partitioning of trace-elements at 900 °C and 2.0 GPa – constraints on the trace-element chemistry of mantle and deep-crustal fluids. *Geochim. Cosmochim. Acta* **59**, 3331–3350.

Brooker R. A. (1998) The effect of CO_2 saturation on immiscibility between silicate and carbonate liquids: an experimental study. *J. Petrol.* **39**, 1905–1915.

Brooker R. A. and Kjarsgaard B. A. (2011) Silicate–carbonate liquid immiscibility and phase relations in the system SiO_2–Na_2O–Al_2O_3–CaO–CO_2 at 0.1–2.5 GPa with applications to carbonatite genesis. *J. Petrol.* **52**, 1281–1305.

Brooker R. A., Kohn S. C., Holloway J. R. and McMillan P. F. (2001) Structural controls on the solubility of CO_2 in silicate melts Part I: bulk solubility data. *Chem. Geol.* **174**, 225–239.

Carr M. J., Feigenson M. D. and Bennett E. A. (1990) Incompatible element and isotopic evidence for tectonic control of source mixing and melt extraction along the Central-American arc. *Contrib. Mineral. Petrol.* **105**, 369–380.

Cervantes P. and Wallace P. J. (2003) Role of H_2O in subduction-zone magmatism: new insights from melt inclusions in high-Mg basalts from central Mexico. *Geology* **31**, 235–238.

Chakrabarti R., Basu A. R., Santo A. P., Tedesco D. and Vaselli O. (2009) Isotopic and geochemical evidence for a heterogeneous mantle plume origin of the Virunga volcanics, Western rift, East African Rift system. *Chem. Geol.* **259**, 273–289.

Chazot G., Menzies M. A. and Harte B. (1996) Determination of partition coefficients between apatite, clinopyroxene, amphibole, and melt in natural spinel lherzolites from Yemen: implications for wet melting of the lithospheric mantle. *Geochim. Cosmochim. Acta* **60**, 423–437.

Chen Y. J., Liu Y. L., Bao J. X., Zhang Z. J., Chen H. Y., Cai W. J. and Helmstaedt H. (2004) Isotopic dating for the volcanic rocks of the Aikendaban formation in the west Tianshan, China and it's tectonic implication. *J. Mineral. Petrol.* **24**, 52–55 (in Chinese with English abstract).

Class C., Altherr R., Volker F., Eberz G. and Mcculloch M. T. (1994) Geochemistry of Pliocene to Quaternary Alkali Basalts from the Huri Hills, Northern Kenya. *Chem. Geol.* **113**, 1–22.

Conceição R. V. and Green D. H. (2004) Derivation of potassic (shoshonitic) magmas by decompression melting of phlogopite+pargasite lherzolite. *Lithos* **72**, 209–229.

Connolly J. A. D. (2005) Computation of phase equilibria by linear programming: a tool for geodynamic modeling and its application to subduction zone decarbonation. *Earth Planet. Sci. Lett.* **236**, 524–541.

Conticelli S., Guarnieri L., Farinelli A., Mattei M., Avanzinelli R., Bianchini G., Boari E., Tommasini S., Tiepolo M., Prelevic D. and Venturelli G. (2009a) Trace elements and Sr–Nd–Pb isotopes of K-rich, shoshonitic, and calc-alkaline magmatism of the Western Mediterranean Region: Genesis of ultrapotassic to calc-alkaline magmatic associations in a post-collisional geodynamic setting. *Lithos* **107**, 68–92.

Conticelli S., Marchionni S., Rosa D., Giordano G., Boari E. and Avanzinelli R. (2009b) Shoshonite and sub-alkaline magmas from an ultrapotassic volcano: Sr–Nd–Pb isotope data on the Roccamonfina volcanic rocks, Roman Magmatic Province, Southern Italy. *Contrib. Mineral. Petrol.* **157**, 41–63.

Coplen T. B., Kendall C. and Hopple J. (1983) Comparison of Stable Isotope Reference Samples. *Nature* **302**, 236–238.

Dalton J. A. and Wood B. J. (1993) The compositions of primary carbonate melts and their evolution through wallrock reaction in the mantle. *Earth Planet. Sci. Lett.* **119**, 511–525.

Dasgupta R. (2013) Ingassing, storage, and outgassing of terrestrial carbon through geologic time. *Rev. Mineral. Geochem.* **75**, 183–229.

Dasgupta R., Hirschmann M. M., McDonough W. F., Spiegelman M. and Withers A. C. (2009) Trace element partitioning between garnet lherzolite and carbonatite at 6.6 and 8.6 GPa with applications to the geochemistry of the mantle and of mantle-derived melts. *Chem. Geol.* **262**, 57–77.

Dasgupta R., Hirschmann M. M. and Smith N. D. (2007) Partial melting experiments of peridotite CO_2 at 3 GPa and genesis of alkalic ocean island basalts. *J. Petrol.* **48**, 2093–2124.

Dasgupta R., Hirschmann M. M. and Withers A. C. (2004) Deep global cycling of carbon constrained by the solidus of anhydrous, carbonated eclogite under upper mantle conditions. *Earth Planet. Sci. Lett.* **227**, 73–85.

Dasgupta R., Mallik A., Tsuno K., Withers A. C., Hirth G. and Hirschmann M. M. (2013) Carbon-dioxide-rich silicate melt in the Earth's upper mantle. *Nature* **493**, 211–215.

de Ignacio C., Munoz M. and Sagredo J. (2012) Carbonatites and associated nephelinites from Sao Vicente, Cape Verde Islands. *Mineral. Mag.* **76**, 311–355.

DePaolo D. J. (1988) *Neodymium Isotope Geochemistry: an Introduction*. Springer-Verlag, Berlin.

Ducea M. N., Saleeby J., Morrison J. and Valencia V. A. (2005) Subducted carbonates, metasomatism of mantle wedges, and possible connections to diamond formation: an example from California. *Am. Mineral.* **90**, 864–870.

Duggen S., Hoernle K., Van den Bogaard P. and Garbe-Schonberg D. (2005) Post-collisional transition from subduction- to intraplate-type magmatism in the westernmost Mediterranean: evidence for continental-edge delamination of subcontinental lithosphere. *J. Petrol.* **46**, 1155–1201.

Elliott T., Plank T., Zindler A., White W. and Bourdon B. (1997) Element transport from slab to volcanic front at the Mariana arc. *J. Geophys. Res.* **102**, 14991–15019.

Foley S. F. (1984) Liquid immiscibility and melt segregation in alkaline lamprophyres from Labrador. *Lithos* **17**, 127–137.

Foley S. F., Venturelli G., Green D. H. and Toscani L. (1987) The ultrapotassic rocks – characteristics, classification, and constraints for petrogenetic models. *Earth-Sci. Rev.* **24**, 81–134.

Frezzotti M. L., Selverstone J., Sharp Z. D. and Compagnoni R. (2011) Carbonate dissolution during subduction revealed by diamond-bearing rocks from the Alps. *Nat. Geosci.* **4**, 703–706.

Gao J. and Klemd R. (2003) Formation of HP-LT rocks and their tectonic implications in the western Tianshan Orogen, NW China: geochemical and age constraints. *Lithos* **66**, 1–22.

Gao J., John T., Klemd R. and Xiong X. M. (2007) Mobilization of Ti–Nb–Ta during subduction: evidence from rutile-bearing dehydration segregations and veins hosted in eclogite, Tianshan, NW China. *Geochim. Cosmochim. Acta* **71**, 4974–4996.

Gao J., Qian Q., Long L., Zhang X., Li J. and Su W. (2009) Accretionary orogenic process of Western Tianshan, China. *Geol. Bull. China* **28**, 1804–1816 (in Chinese with English abstract).

Giampaolo C., Godano R. F., DiSabatino B. and Barrese E. (1997) The alteration of leucite-bearing rocks: a possible mechanism. *Eur. J. Mineral.* **9**, 1277–1291.

Goldstein S. L., Onions R. K. and Hamilton P. J. (1984) A Sm–Nd isotopic study of atmospheric dusts and particulates from major river systems. *Earth Planet. Sci. Lett.* **70**, 221–236.

Gorman P. J., Kerrick D. M. and Connolly J. A. D. (2006) Modeling open system metamorphic decarbonation of subducting slabs. *Geochem. Geophys. Geosyst.* **7**.

Guo Z. F., Wilson M., Liu J. Q. and Mao Q. (2006) Post-collisional, potassic and ultrapotassic magmatism of the northern Tibetan Plateau: constraints on characteristics of the mantle source, geodynamic setting and uplift mechanisms. *J. Petrol.* **47**, 1177–1220.

Guzmics T., Mitchell R. H., Szabo C., Berkesi M., Milke R. and Ratter K. (2012) Liquid immiscibility between silicate, carbonate and sulfide melts in melt inclusions hosted in co-precipitated minerals from Kerimasi volcano (Tanzania): evolution of carbonated nephelinitic magma. *Contrib. Mineral. Petrol.* **164**, 101–122.

Hamilton D. L., Freestone I. C., Dawson J. B. and Donaldson C. H. (1979) Origin of carbonatites by liquid immiscibility. *Nature* **279**, 52–54.

Hart S. R. (1984) A large-scale isotope anomaly in the southern-Hemisphere mantle. *Nature* **309**, 753–757.

Hart S. R. and Aldrich L. T. (1967) Fractionation of potassium/rubidium by amphiboles: implications regarding mantle composition. *Science* **155**, 325–327.

Hermann J. and Rubatto D. (2009) Accessory phase control on the trace element signature of sediment melts in subduction zones. *Chem. Geol.* **265**, 512–526.

Hoernle K., Tilton G., Le Bas M. J., Duggen S. and Garbe-Schonberg D. (2002) Geochemistry of oceanic carbonatites compared with continental carbonatites: mantle recycling of oceanic crustal carbonate. *Contrib. Mineral. Petrol.* **142**, 520–542.

Hofmann A. W. (1997) Mantle geochemistry: the message from oceanic volcanism. *Nature* **385**, 219–229.

Iacovino K., Moore G., Roggensack K., Oppenheimer C. and Kyle P. (2013) H_2O–CO_2 solubility in mafic alkaline magma: applications to volatile sources and degassing behavior at Erebus volcano, Antarctica. *Contrib. Mineral. Petrol.* **166**, 845–860.

Ionov D. A. and Hofmann A. W. (1995) Nb–Ta-rich mantle amphiboles and micas – implications for subduction-related metasomatic trace-element fractionations. *Earth Planet. Sci. Lett.* **131**, 341–356.

Jacobsen S. B. and Wasserburg G. J. (1980) Sm–Nd isotopic evolution of chondrites. *Earth Planet. Sci. Lett.* **50**, 139–155.

Jenner F. E., Bennett V. C., Nutman A. P., Friend C. R. L., Norman M. D. and Yaxley G. (2009) Evidence for subduction at 3.8 Ga: geochemistry of arc-like metabasalts from the southern edge of the Isua Supracrustal Belt. *Chem. Geol.* **261**, 82–97.

Jiang Y. H., Jiang S. Y., Dai B. Z., Liao S. Y., Zhao K. D. and Ling H. F. (2009) Middle to late Jurassic felsic and mafic magmatism in southern Hunan province, southeast China: implications for a continental arc to rifting. *Lithos* **107**, 185–204.

Kessel R., Schmidt M. W., Ulmer P. and Pettke T. (2005) Trace element signature of subduction-zone fluids, melts and supercritical liquids at 120–180 km depth. *Nature* **437**, 724–727.

Klemme S. and O'Neill H. S. (2000) The near-solidus transition from garnet lherzolite to spinel lherzolite. *Contrib. Mineral. Petrol.* **138**, 237–248.

Kogarko L. N., Henderson C. M. B. and Pacheco H. (1995) Primary Ca-rich carbonatite magma and carbonate–silicate–sulfide liquid immiscibility in the upper-mantle. *Contrib. Mineral. Petrol.* **121**, 267–274.

Kogiso T., Tatsumi Y. and Nakano S. (1997) Trace element transport during dehydration processes in the subducted oceanic crust.1. Experiments and implications for the origin of ocean island basalts. *Earth Planet. Sci. Lett.* **148**, 193–205.

Labanieh S., Chauvel C., Germa A. and Quidelleur X. (2012) Martinique: a clear case for sediment melting and slab dehydration as a function of distance to the trench. *J. Petrol.* **53**, 2441–2464.

Lebas M. J., Lemaitre R. W., Streckeisen A. and Zanettin B. (1986) A chemical classification of volcanic-rocks based on the total alkali silica diagram. *J. Petrol.* **27**, 745–750.

Lee C. T., Rudnick R. L., McDonough W. F. and Horn I. (2000) Petrologic and geochemical investigation of carbonates in peridotite xenoliths from northeastern Tanzania. *Contrib. Mineral. Petrol.* **139**, 470–484.

Lee W. J. and Wyllie P. J. (1997) Liquid immiscibility between nephelinite and carbonatite from 1.0 to 2.5 GPa compared with mantle melt compositions. *Contrib. Mineral. Petrol.* **127**, 1–16.

Leeman W. P., Carr M. J. and Morris J. D. (1994) Boron geochemistry of the Central-American volcanic arc – constraints on the genesis of subduction-related magmas. *Geochim. Cosmochim. Acta* **58**, 149–168.

Lesne P., Scaillet B., Pichavant M. and Beny J. M. (2011) The carbon dioxide solubility in alkali basalts: an experimental study. *Contrib. Mineral. Petrol.* **162**, 153–168.

Li H. Q., Zhou S. and Cai H. (1997) Chronology of mineralization of the nileike copper deposit in northern Xinjian. *Acta Geosci. Sin.* **18**, 185–187 (in Chinese with English abstract).

Li X. H. (1997) Geochemistry of the Longsheng Ophiolite from the southern margin of Yangtze Craton, SE China. *Geochem. J.* **31**, 323–337.

Li X. H., Qi C. S., Liu Y., Liang X. R., Tu X. L., Xie L. W. and Yang Y. H. (2005) Petrogenesis of the Neoproterozoic bimodal volcanic rocks along the western margin of the Yangtze Block: new constraints from Hf isotopes and Fe/Mn ratios. *Chin. Sci. Bull.* **50**, 2481–2486.

Liang X. R., Wei G. J., Li X. H. and Liu Y. (2003) Precise determination of $^{143}Nd/^{144}Nd$ and Sm/Nd ratios using multiple-collector inductively coupled plasmamass spectrometer (MC-ICPMS). *Geochimica* **32**, 91–96 (in Chinese with English abstract).

Lin P. N., Stern R. J., Morris J. and Bloomer S. H. (1990) Nd-isotopic and Sr-isotopic compositions of lavas from the Northern Mariana and Southern Volcano arcs – implications for the origin of island-arc melts. *Contrib. Mineral. Petrol.* **105**, 381–392.

Liu Y., Liu H. C. and Li X. H. (1996) Simultaneous and precise determination of 40 trace elements in rock samples using ICP-MS. *Geochimica* **25**, 552–558.

Lugmair G. W. and Marti K. (1978) Lunar initial $^{143}Nd/^{144}Nd$: differential evolution of the lunar crust and mantle. *Earth Planet. Sci. Lett.* **39**, 349–357.

Luhr J. F., Arandagomez J. J. and Housh T. B. (1995) San-quintin volcanic field, Baja-California-Norte, Mexico – geology, petrology, and geochemistry. *J. Geophys. Res.* **100**, 10353–10380.

Luo Y., Niu H. C., Shan Q., Zhang B., Zhou C. P., Yang W. B. and Yu X. Y. (2009) Discovery of the basaltic andesite-high-K basaltic andesite–trachyandesite association in the Yuximolegai Daban, West Tianshan and its geological significance. *Acta Petrol. Sin.* **25**, 934–943 (in Chinese with English abstract).

Marin-Ceron M. I., Moriguti T., Makishima A. and Nakamura E. (2010) Slab decarbonation and CO_2 recycling in the Southwestern Colombian volcanic arc. *Geochim. Cosmochim. Acta* **74**, 1104–1121.

Marty B. and Tolstikhin I. N. (1998) CO_2 fluxes from mid-ocean ridges, arcs and plumes. *Chem. Geol.* **145**, 233–248.

McCulloch M. T. and Black L. P. (1984) Sm–Nd isotopic systematics of Enderby Land granulites and evidence for the redistribution of Sm and Nd during metamorphism. *Earth Planet. Sci. Lett.* **71**, 46–58.

Mourtada S., LeBas M. J. and Pin C. (1997) Petrogenesis of Mg-carbonatites from Tamazert in the Moroccan High Atlas. *C. R. Acad. Sci. II. A.* **325**, 559–564.

Patino L. C., Carr M. J. and Feigenson M. D. (2000) Local and regional variations in Central American arc lavas controlled by variations in subducted sediment input. *Contrib. Mineral. Petrol.* **138**, 265–283.

Phillips W. J. (1973) Interpretation of crystalline spheroidal structures in igneous rocks. *Lithos* **6**, 235–244.

Pilet S., Baker M. B. and Stolper E. M. (2008) Metasomatized lithosphere and the origin of alkaline lavas. *Science* **320**, 916–919.

Pirajno F., Seltmann R. and Yang Y. (2011) A review of mineral systems and associated tectonic settings of northern Xinjiang, NW China. *Geosci. Front.* **2**, 157–185.

Plank T. and Langmuir C. H. (1998) The chemical composition of subducting sediment and its consequences for the crust and mantle. *Chem. Geol.* **145**, 325–394.

Polat A. and Hofmann A. W. (2003) Alteration and geochemical patterns in the 3.7–3.8 Ga Isua greenstone belt, West Greenland. *Precambrian Res.* **126**, 197–218.

Poli S., Franzolin E., Fumagalli P. and Crottini A. (2009) The transport of carbon and hydrogen in subducted oceanic crust: an experimental study to 5 GPa. *Earth Planet. Sci. Lett.* **278**, 350–360.

Putnis C. V., Geisler T., Schmid-Beurmann P., Stephan T. and Giampaolo C. (2007) An experimental study of the replacement of leucite by analcime. *Am. Mineral.* **92**, 19–26.

Pyle J. M. and Haggerty S. E. (1994) Silicate–carbonate liquid immiscibility in upper-mantle eclogites – implications for natrosilicic and carbonatitic conjugate melts. *Geochim. Cosmochim. Acta* **58**, 2997–3011.

Ray J. S., Ramesh R. and Pande K. (1999) Carbon isotopes in Kerguelen plume-derived carbonatites: evidence for recycled inorganic carbon. *Earth Planet. Sci. Lett.* **170**, 205–214.

Rudnick R. L., Mcdonough W. F. and Chappell B. W. (1993) Carbonatite metasomatism in the northern Tanzanian mantle – petrographic and geochemical characteristics. *Earth Planet. Sci. Lett.* **114**, 463–475.

Sano Y. and Williams S. N. (1996) Fluxes of mantle and subducted carbon along convergent plate boundaries. *Geophys. Res. Lett.* **23**, 2749–2752.

Shan Q., Zhang B., Luo Y., Zhou C. P., Yu X. Y., Zeng Q. S., Yang W. B. and Niu H. C. (2009) Characteristics and trace element geochemistry of pyrite from the Songhu iron deposit, Nilek County, Xinjiang, China. *Acta Petrol. Sin.* **25**, 1456–1464.

Skora S. and Blundy J. (2010) High-pressure hydrous phase relations of radiolarian clay and implications for the involvement of subducted sediment in arc magmatism. *J. Petrol.* **51**, 2211–2243.

Sleep N. H. and Zahnle K. (2001) Carbon dioxide cycling and implications for climate on ancient Earth. *J. Geophys. Res.* **106**, 1373–1399.

Sokolov S. (2002) Melt inclusions as indicators of the magmatic origin of carbonatite rare metal and rare earth minerals. *Chem. Geol.* **183**, 373–378.

Solovova I. P. and Girnis A. V. (2012) Silicate–carbonate liquid immiscibility and crystallization of carbonate and K-rich

basaltic magma: insights from melt and fluid inclusions. *Mineral. Mag.* **76**, 411–439.
Spandler C. and Pirard C. (2013) Element recycling from subducting slabs to arc crust: a review. *Lithos* **170**, 208–223.
Steiger R. H. and Jäger E. (1977) Subcommission on geochronology: convention on the use of decay constants in geo- and cosmochronology. *Earth Planet. Sci. Lett.* **36**, 359–362.
Stoppa F., Rosatelli G., Wall F. and Jeffries T. (2005) Geochemistry of carbonatite–silicate pairs in nature: a case history from Central Italy. *Lithos* **85**, 26–47.
Sun H., Xiao Y., Gao Y., Lai J., Hou Z. and Wang Y. (2013) Fluid and melt inclusions in the Mesozoic Fangcheng basalt from North China Craton: implications for magma evolution and fluid/melt-peridotite reaction. *Contrib. Mineral. Petrol.* **165**, 885–901.
Sun L. H., Wang Y. J., Fan W. M. and Zi J. W. (2008) Post-collisional potassic magmatism in the Southern Awulale Mountain, western Tianshan Orogen: petrogenetic and tectonic implications. *Gondwana Res.* **14**, 383–394.
Sun S. S. and McDonough W. F. (1989) Chemical and isotopic systematics of oceanic basalts: implications for mantle composition and process. In *Magmatism in Oceanic Basins*, vol. 42 (eds. A. D. Saunders and M. J. Norry). Geol. Soc. Sp. Publ., pp. 313–345.
Sweeney R. J. (1994) Carbonatite melt compositions in the Earth's mantle. *Earth Planet. Sci. Lett.* **128**, 259–270.
Syracuse E. M. and Abers G. A. (2006) Global compilation of variations in slab depth beneath arc volcanoes and implications. *Geochem. Geophys. Geosyst.* **7**.
Syracuse E. M., van Keken P. E. and Abers G. A. (2010) The global range of subduction zone thermal models. *Phys. Earth Planet. Int.* **183**, 73–90.
Tappe S., Foley S. F., Jenner G. A., Heaman L. M., Kjarsgaard B. A., Romer R. L., Stracke A., Joyce N. and Hoefs J. (2006) Genesis of ultramafic lamprophyres and carbonatites at Aillik Bay, Labrador: a consequence of incipient lithospheric thinning beneath the North Atlantic craton. *J. Petrol.* **47**, 1261–1315.
Taylor H. P., Frechen J. and Degens E. T. (1967) Oxygen and carbon isotope studies of carbonatites from the Laacher See District, West Germany and the Alnö District, Sweden. *Geochim. Cosmochim. Acta* **31**, 407–430.
Thomsen T. B. and Schmidt M. W. (2008) Melting of carbonated pelites at 2.5–5.0 GPa, silicate–carbonatite liquid immiscibility, and potassium–carbon metasomatism of the mantle. *Earth Planet. Sci. Lett.* **267**, 17–31.
Tilton G. R., Bryce J. G. and Mateen A. (1998) Pb–Sr–Nd isotope data from 30 and 300 Ma collision zone carbonatites in Northwest Pakistan. *J. Petrol.* **39**, 1865–1874.
Tsuno K. and Dasgupta R. (2012) The effect of carbonates on near-solidus melting of pelite at 3 GPa: relative efficiency of H_2O and CO_2 subduction. *Earth Planet. Sci. Lett.* **319**, 185–196.
Turner S. and Hawkesworth C. (1997) Constraints on flux rates and mantle dynamics beneath island arcs from Tonga-Kermadec lava geochemistry. *Nature* **389**, 568–573.
van Achterbergh E., Griffin W. L., Ryan C. G., O'Reilly S. Y., Pearson N. J., Kivi K. and Doyle B. J. (2002) Subduction signature for quenched carbonatites from the deep lithosphere. *Geology* **30**, 743–746.
Varekamp J. C., Kreulen R., Poorter R. P. E. and Vanbergen M. J. (1992) Carbon-sources in arc volcanism, with implications for the carbon-cycle. *Terra Nova* **4**, 363–373.
Veksler I. V., Dorfman A. M., Dulski P., Kamenetsky V. S., Danyushevsky L. V., Jeffries T. and Dingwell D. B. (2012) Partitioning of elements between silicate melt and immiscible fluoride, chloride, carbonate, phosphate and sulfate melts, with implications to the origin of natrocarbonatite. *Geochim. Cosmochim. Acta* **79**, 20–40.
Veksler I. V., Petibon C., Jenner G. A., Dorfman A. M. and Dingwell D. B. (1998) Trace element partitioning in immiscible silicate–carbonate liquid systems: an initial experimental study using a centrifuge autoclave. *J. Petrol.* **39**, 2095–2104.
Wallace M. E. and Green D. H. (1988) An experimental-determination of primary carbonatite magma composition. *Nature* **335**, 343–346.
Wallace P. J. (2005) Volatiles in subduction zone magmas: concentrations and fluxes based on melt inclusion and volcanic gas data. *J. Volcanol. Geotherm. Res.* **140**, 217–240.
Walter M. J., Bulanova G. P., Armstrong L. S., Keshav S., Blundy J. D., Gudfinnsson G., Lord O. T., Lennie A. R., Clark S. M., Smith C. B. and Gobbo L. (2008) Primary carbonatite melt from deeply subducted oceanic crust. *Nature* **454**, U622–U630.
Wang B., Shu L. S., Faure M., Jahn B. M., Cluzel D., Charvet J., Chung S. L. and Meffre S. (2011) Paleozoic tectonics of the southern Chinese Tianshan: insights from structural, chronological and geochemical studies of the Heiyingshan ophiolitic melange (NW China). *Tectonophysics* **497**, 85–104.
Watkinson D. H. and Wyllie P. J. (1971) Experimental study of the composition join $NaAlSiO_4$–$CaCO_3$–H_2O and the genesis of alkalic rock – carbonatite complexes. *J. Petrol.* **12**, 357–378.
Wei G. J., Liang X. R., Li X. H. and Liu Y. (2002) Precise measurement of Sr isotopic of liquid and solid base using (LP)MC-ICPMS. *Geochimica* **31**, 295–299 (in Chinese with English abstract).
Woolley A. R. (2003) Igneous silicate rocks associated with carbonatites: their diversity, relative abundances and implications for carbonatite genesis. *Periodico di Mineralogia* **72**, 9–17.
Xiao W., Windley B. F., Allen M. B. and Han C. (2013) Paleozoic multiple accretionary and collisional tectonics of the Chinese Tianshan orogenic collage. *Gondwana Res.* **23**, 1316–1341.
Xiao W. J., Han C. M., Yuan C., Sun M., Zhao G. C. and Shan Y. H. (2010) Transitions among Mariana-, Japan-, Cordillera- and Alaska-type arc systems and their final juxtapositions leading to accretionary and collisional orogenesis. *Geol. Soc. Sp. Publ.* **338**, 35–53.
Yang W. B., Niu H. C., Shan Q., Luo Y., Sun W. D., Li C. Y., Li N. B. and Yu X. Y. (2012) Late Paleozoic calc-alkaline to shoshonitic magmatism and its geodynamic implications, Yuximolegai area, western Tianshan, Xinjiang. *Gondwana Res.* **22**, 325–340.
Yang X., Zhang L. F., Tian Z. L. and Bader T. (2013) Petrology and U–Pb zircon dating of coesite-bearing metapelite from the Kebuerte Valley, western Tianshan, China. *J. Asian Earth Sci.* **70–71**, 295–307.
Yaxley G. M., Crawford A. J. and Green D. H. (1991) Evidence for carbonatite metasomatism in spinel peridotite xenoliths from western Victoria, Australia. *Earth Planet. Sci. Lett.* **107**, 305–317.
Zack T. and John T. (2007) An evaluation of reactive fluid flow and trace element mobility in subducting slabs. *Chem. Geol.* **239**, 199–216.
Zeng G., Chen L. H., Xu X. S., Jiang S. Y. and Hofmann A. W. (2010) Carbonated mantle sources for Cenozoic intra-plate alkaline basalts in Shandong, North China. *Chem. Geol.* **273**, 35–45.
Zhang H. F. (2005) Transformation of lithospheric mantle through peridotite-melt reaction: a case of Sino-Korean craton. *Earth Planet. Sci. Lett.* **237**, 768–780.
Zhang H. F., Nakamura E., Sun M., Kobayashi K., Zhang J., Ying J. F., Tang Y. J. and Niu L. F. (2007) Transformation of subcontinental lithospheric mantle through peridotite-melt

reaction: evidence from a highly fertile mantle xenolith from the north China Craton. *Int. Geol. Rev.* **49**, 658–679.

Zhang L., Ellis D. J., Arculus R. J., Jiang W. and Wei C. (2003) 'Forbidden zone' subduction of sediments to 150 km depth – the reaction of dolomite to magnesite plus aragonite in the UHPM metapelites from western Tianshan, China. *J. Metamorph. Geol.* **21**, 523–529.

Zhang L. F., Ellis D. J. and Jiang W. B. (2002a) Ultrahigh-pressure metamorphism in western Tianshan, China: Part I. Evidence from inclusions of coesite pseudomorphs in garnet and from quartz exsolution lamellae in omphacite in eclogites. *Am. Mineral.* **87**, 853–860.

Zhang L. F., Ellis D. J., Williams S. and Jiang W. B. (2002b) Ultrahigh pressure metamorphism in western Tianshan, China: Part II. Evidence from magnesite in eclogite. *Am. Mineral.* **87**, 861–866.

Zhang P. F., Tang Y. J., Hu Y., Zhang H. F., Su B. X., Xiao Y. and Santosh M. (2012a) Review of melting experiments on carbonated eclogite and peridotite: insights into mantle metasomatism. *Int. Geol. Rev.* **54**, 1443–1455.

Zhang X., Tian J. Q., Gao J., Klemd R., Dong L. H., Fan J. J., Jiang T., Hu C. J. and Qian Q. (2012b) Geochronology and geochemistry of granitoid rocks from the Zhibo syngenetic volcanogenic iron ore deposit in the Western Tianshan Mountains (NW-China): constraints on the age of mineralization and tectonic setting. *Gondwana Res.* **22**, 585–596.

Zhao Z. H., Xiong X. L., Wang Q., Bai Z. H. and Qiao Y. L. (2009) Late Paleozoic underplating in North Xinjiang: evidence from shoshonites and adakites. *Gondwana Res.* **16**, 216–226.

Zhu B. Q., Zhang J. L., Tu X. L., Chang X. Y., Fan C. Y., Liu Y. and Liu J. Y. (2001) Pb, Sr, and Nd isotopic features in organic matter from China and their implications for petroleum generation and migration. *Geochim. Cosmochim. Acta* **65**, 2555–2570.

Zhu Y. F., Guo X., Song B., Zhang L. F. and Gu L. B. (2009) Petrology, Sr–Nd–Hf isotopic geochemistry and zircon chronology of the Late Palaeozoic volcanic rocks in the southwestern Tianshan Mountains, Xinjiang, NW China. *J. Geol. Soc. London* **166**, 1085–1099.

Zhu Y. F., Zhou J., Song B., Zhang L. F. and Guo X. (2006) Age of the "Dahalajunshan" Formation in Xinjiang and its disintegration. *Geology in China* **33**, 488–498 (in Chinese with English abtract).

Associate editor: Weidong Sun